We highly appreciate helpful comments and suggestions by both reviewers. In the following, the comments by reviewers are underlined and our responses to the comments are in normal characters. Modifications to the text are shown in quotation marks with bold characters indicating newly added text, and normal characters indicating text that was already present in the previous version. The line numbering is referenced to the marked-up manuscript version.

Interactive comment on "Sea–ice and water dynamics and moonlight impact the acoustic backscatter diurnal signal over the eastern Beaufort Sea continental slope" by Igor A. Dmitrenko et al. by Jørgen Berge (Referee)

1. Abstract: To which degree will the ADCP "see" suspended particles? Is it really true that suspended particles can mask the backscatter signal from zooplankton? I think this should be included in the discussion as a separate topic

There is a large number of papers demonstrating that the sound wave is scattered off the particles, and the backscatter intensity is related to suspended sediment concentration. Over the past few decades, the implication of ADCPs for detection of suspended sediment became commonly accepted (e.g., see overview by Thorne and Hurther, 2014: An overview on the use of backscattered sound for measuring suspended particle size and concentration profiles in non-cohesive inorganic sediment transport studies, doi:10.1016/j.csr.2013.10.017). Nowadays ADCPs (including those operating at 300 KHz) are extensively used for suspended sediment transport monitoring (e.g., Venditti et al., 2016, doi:10.1002/2015WR017348; Dwinovantyo et al., 2017, doi:10.1155/2017/4890421; etc. etc.). Moreover, in 2007, RDI published a technical note providing information on commercially available software packages converting ADCP backscatter data into total suspended sediment concentration as follows: http://www.teledynemarine.com/Documents/Brand%20Support/RD%20INSTRUMENTS/Technical%20Resources/Technical%20Notes/WorkHorse%20-%20ADCP%20Special%20Applications%20and%20Modes/FST017.pdf. Therefore, there is no doubt that ADCPs "see" suspended particles. So, we do not think that discussion on this point is appropriate in the context of our manuscript. Discussion on how the backscatter signal from zooplankton is impacted by suspended particles is already provided in the last paragraph of section 6.1 (lines 590-604). Figures 7d-7f clearly show enhanced MVBS 24 h a day, which is consistent with an acoustic signature of suspended particles. The light attenuation enhanced by suspended particles likely impacts DVM during summer 2005. We agree that term "mask" seems to be inappropriate in this context. DVM can also be impacted by light attenuation generated by enhanced concentration of suspended particles in water column. So, following this comment we changed "*masked*" to "***impacted***" (lines 20, 282, and 590).

2. Introduction: Line 45: Zooplankton samples taken 13 years after the mooring was deployed? I would suggest that the part on zooplankton samples is taken out, as it in reality have very little added value. This applies throughout the manuscript

The part on zooplankton samples was removed, lines 135-149.

3. Line 46: "The environmental factors controlling DVM in the seasonally ice-covered Arctic areas,..., remains poorly assessed". There have been numerous studies documenting that it is light that is proximate cue for DVM, both in the Arctic and elsewhere. So if you mean that proximate cues are poorly studied, I would disagree. However, if you are referring to other environmental factor and their effect on DVM, then this is a topic not merely poorly studied in the Arctic, but in general. The effect of upwelling/downwelling is also a novel and important contribution to the understanding of DVM in general! I would recommend rewriting this so that it becomes clearer?

Reviewer #1 is correct. To make our statement clearer, we modified this sentence in line 46 as follows: "*The **oceanographic** factors controlling DVM in the seasonally ice-covered Arctic areas... remains poorly assessed*".

4. Line 48: To avoid confusion, I would refer to Cohen et al 2020 (table 3.1) with definition of polar night...since you are discussing light levels, the most correct term is actually "civil twilight" which occur during polar twilight when the sun is less than 6 degrees below the horizon. The same applies for the other locations mentioned in the sentences below (need to separate between the definition of types of twilight and polar night periods)

Following this comment, we modified text in lines 48-54 as follows: "***At t**his latitude **no actual daylight is experienced during short winter daylight hours with the exception of the civil twilight** when solar illumination is still sufficient for the human eye to distinguish terrestrial objects. This geographical position makes our DVM observational site vastly different from those at Svalbard (**astronomical twilight, the Sun is between 12 and 18° below the horizon**, ~80°N; e.g., Grenvald et al., 2016; Darnis et al., 2017), Canada Basin (nautical twilight, the Sun is between 6 and 12° below the horizon, ~77.5°N; La et al., 2018), and Northeast Greenland (nautical twilight, ~74.5°N, Petrusevich et al., 2016)*".

5. Data: Line 83-100: Wallace et al 2010 and later Hobbs et al 2018 used and published a procedure on how to infer ice-cover from an upward-looking ADCP. This would provide a good and in situ data source for ice cover at the mooring site

We estimate the sea-ice cover concentration from AMSR-E. Following comment #8 by Reviewer #2, we changed sea ice concentrations, spatially-averaged over a 200-km rectangle, to that for the single pixel, closest to the mooring position (please see revised text in lines 91-94). The sea-ice thickness, however, remained uncertain. A procedure on how to infer ice-cover thickness from an upward-looking ADCP suggested by Wallace et al. (2010) and later by Hobbs et al. (2018) is based on the algorithm published by Hyatt et al. (2008, doi: 10.1016/j.dsr2.2007.11.004). According to that algorithm, the ADCP bin that samples the sea surface or sea-ice bottom is identified as the bin above the bin with maximum backscatter intensity (Hyatt et al, 2008). For CA13, the velocity and acoustic backscatter data were obtained at 8-m depth intervals, so the last sampled bin #13 was at 4 m depth. This level corresponds to the maximum backscatter intensity (as shown in the figure presented below). Thus, there is no bin above the one with the maximum backscatter intensity, which does not allow to apply this algorithm. To resolve this issue, we followed a recommendation provided by Reviewer #2 (his/her comment #2) to derive sea-ice thickness from the Pan-Arctic Ice Ocean Modeling and Assimilation System (PIOMAS) and Hybrid Coordinate Ocean Model (HYCOM) + Community Ice Code (CICE) coupled ocean and sea ice system. Instead of the mean seasonal cycle, we used grid daily data from PIOMAS and HYCOM+CICE for the grid node closest to the mooring position (please see revised text in lines 103-119).

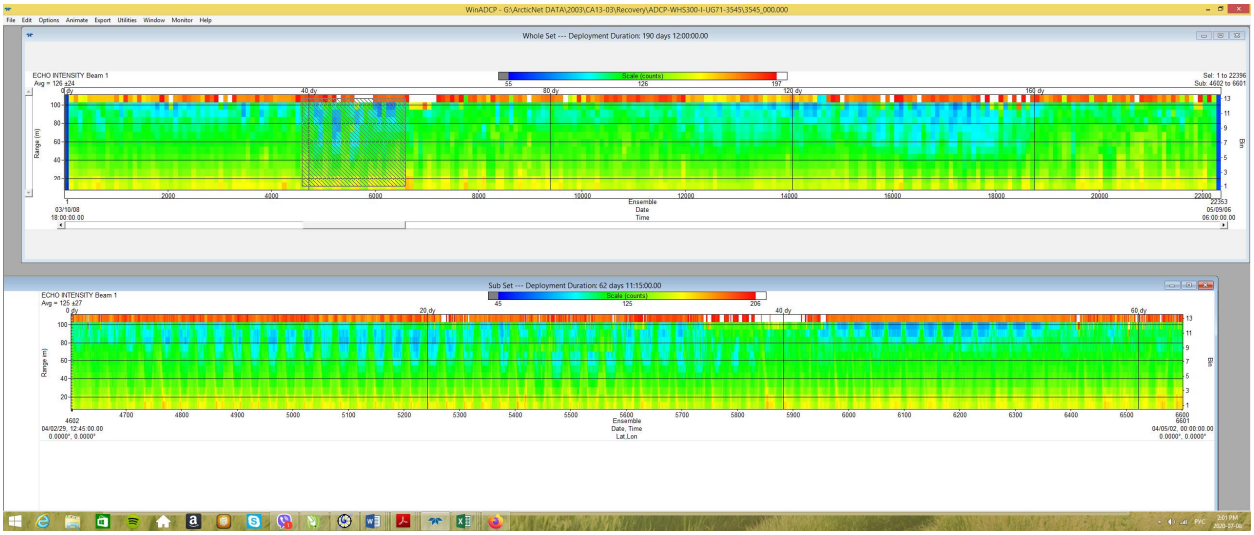

Figure shows acoustic backscatter data from a 300 kHz upward-looking Workhorse Sentinel ADCP by RDI deployed at CA13

6. Lines 101-115: I would argue that this part should be deleted. The samples were collected no less than 13 years after the mooring was deployed, and actually relatively far away from the mooring site. There need to be some seriously strong arguments (that are not provided) for using these samples as a reference point for which scatterers were present 11-13 year earlier. The strength of the manuscript is NOT decreased by omitting these data (quite the opposite, I would argue) - much of the discussion is still valid without referring to zooplankton nets taken in September 2016.

The part on zooplankton samples was omitted in lines 135-149, 458-466, and 489-515. Figure 1 was modified accordingly, and Figure 10 was removed.

7. Lines 201-206: Check values...disregarding atmospheric refraction, the polar day and polar night are symmetrical. Atmospheric refraction will prolong the observed polar day, but hardly as much as presented here (20 days longer polar day compared to the polar night).

The duration of polar night and polar day (the Sun 24 h a day below and above the horizon, respectively) for CA13 position (71°21.356'N, 228°38.176'E) was taken from https://nrc.canada.ca/en/research-development/products-services/software-applications/sun-calculator/. The NOAA calculator at https://www.esrl.noaa.gov/gmd/grad/solcalc/sunrise.html provides similar results. For the North Pole location, this calculator gives results on the duration of the Polar Night and the midnight sun that are similar to those in your Figure 1.5 caption, page 12, POLAR NIGHT Marine Ecology: Life and Light in the Dead of Night, 2020. Following comment #17 by Reviewer #2, this text was shortened and moved to lines 54-57.

8. Discussion Line 438-440: DVM during the polar night is most likely not "diurnal movement of zooplankton towards the surface at dusk", but rather the opposite (movement away for the surface during the short period of increased illumination at around noon). Suttle, but important distinction in order to understand the process of DVM during the polar night (see recent literature on polar night zooplankton and dvm)

The text in lines 517-525 discusses results on DVM at CA13 with respect to the illuminance threshold. During the polar night, these results clearly show the diurnal movement of zooplankton toward the surface at dusk (higher MVBS highlighted by green color in Figure 7d), and descends back the next morning before the short period of increased illumination at around noon (lower MVBS highlighted by dark blue color in Figure 7d). With respect to the reversed DVM (movement away for the surface during the short period of increased illumination at around noon during the Polar Night), Reviewer #1 likely referenced observations taken during the astronomical twilight at 79-80°N (e.g., Berge et al., 2008; Wallace et al., 2010), where during the civil polar night the Sun is between 12° and 18° below the horizon. In contrast, we used observations taken during the civil twilight, when the Sun was between 0 and <6° below the horizon. We pointed out this important difference in lines 51-54: "*This geographical position makes our DVM observational site vastly different from those at Svalbard (**astronomical twilight, the Sun is between 12 and 18° below the horizon**, ~80°N; e.g., Grenvald et al., 2016; Darnis et al., 2017), Canada Basin (**nautical twilight, the Sun is between 6 and 12° below the horizon**, ~77.5°N; La et al., 2018), and Northeast Greenland (**nautical twilight**, ~74.5°N, Petrusevich et al., 2016)*".

9. Section 7.4: How does this study deviate from previous studies (e.g. from Svalbard) that have aimed at studying the effect of water masses, halo- and pycnoclines, etc?

The previous studies from the Svalbard area were focused on the relationship between zooplankton community structure and the local hydrography (e.g. Willis et al., 2008, 2011; Kwasniewski et al., 2012; Berge et al., 2014). In contrast, Section 6.3 (former section 7.4) is focused on the DVM modifications related to water dynamics. Effects of water masses and stratification were not discussed because only limited CTD information is available at CA13.

10. General comment: I find the results in relation to an absolute threshold of light (lux=1) interesting, but I think the authors have a lot to gain from presenting a more thorough discussion on the importance of light intensity vs rate of change. Most published papers emphasise the rate of change as the important cue. Also, the use of lux is not very common in studies of DVM - is it possible to relate lux to absolute quantas of photons? This would enhance comparison with previous studies.

"Our results on the light threshold are consistent with the preferendum (isolume) hypothesis (e.g., Cohen and Forward, 2009). A variant of the preferendum hypothesis, the absolute intensity threshold hypothesis, suggests that an ascent at sunset is initiated once the light intensity decreases below a particular threshold level and a descent at sunrise occurs when the light intensity increases above the threshold intensity (e.g., Cohen and Forward, 2019). This is in line with our findings on an absolute 0.1-lux threshold of light, which corresponds to the moonlight illuminance at the gibbous moon during clear sky (Gaston et al., 2014)". We added this statement in lines 525-530. We introduced an artificial visual boundary on the illuminance colour scheme at 1 lux (gray to orange), which corresponds to illuminance during the deep twilight – lines 177-179. For the sunlight, 1 lux corresponds to about 0.019 micromoles photons per square meter per second (µmole photons m^{-2} s^{-1}). Following this comment, we introduced this unit for the color scale of the under-ice illuminance in Figures 3c-3e.

Interactive comment on "Sea–ice and water dynamics and moonlight impact the acoustic backscatter diurnal signal over the eastern Beaufort Sea continental slope" by Igor A. Dmitrenko et al.

Anonymous Referee #2

This paper describes diurnal vertical migration of zooplankton and associated changes in acoustic backscatter intensity measured in the eastern Beaufort Sea in response to daily cycles in light illuminance. Undoubtedly, this study provides a valuable insight into how the polar ecosystem evolves in response to the light cycle and is of interest for polar biologists and oceanographers. However, the manuscript in its present form has many flaws and therefore needs major revision. In several places, the text is not well structured and clearly written. The results and discussion are not well separated and include numerous repetitions of the same content in many places. I would recommend the authors revise their text to improve its clarity. Further, I provided my suggestions as to what improvements are needed before this paper may be accepted.

General comments:

1. The logical link between evaluation of zooplankton communities and DVM at the mooring in 2003-2005 looks weak. This section and further discussion are entirely based on biological samplings collected in 2016 and separated from the time of mooring observations by more than eleven years. This is a considerably long period. I am surprised that the authors push us to believe that nothing happened with zooplankton communities in the Beaufort Sea over this time. It is unlikely that this is true, especially if we all know about substantial changes taking place in almost all components of the Arctic climate system during this time. I'm not claiming that any new biological species appear at the mooring site even if it might be the case, but it's tough to believe, for instance, that the biomass of each identified class remains unchanged. This raises the question how the presented materials correspond to the conditions at the mooring in 2003? Moreover, zooplankton samples in 2016 were collected for one particular month and, thus, cannot be representative for the entire seasonal cycle, making this part even more speculative. The authors are entirely mute about all these uncertainties. I would suggest the authors either improve that part providing more arguments for why we should trust this analysis or completely remove it.

This section in lines 135-149, 458-466, and 489-515 was completely omitted, also following recommendations #2 and #6 by Reviewer #1. Figure 1 was modified accordingly, and Figure 10 was removed.

2. An additional concern arises about sea-ice data. The authors do not really have at hand an appropriate sea ice thickness record to examine its impact on annual changes of zooplankton DVM. Instead, for simulations, they used a mean seasonal cycle of ice thickness that cannot represent natural year-to-year variability at the CA13 mooring. Thus, the comparison of ice impact on the simulated illuminance in 2004 and 2005 looks questionable. The use of the complementary ICESat data set partially tones down this problem, but does not address it in details because these data are also constrained. In that situation, the option I suggest is to rely on available models like PIOMAS, for example, or other ocean reanalyses data, which assimilate ice concentrations and thicknesses measurements. In that case, the discussion of ice impact on DVM may be more straightforward.

Following this comment, the sea-ice description in the manuscript was extensively improved and extended. As part of responding to this comment, we completely removed a mean seasonal cycle of ice thickness by Melling et al. (2005) and Krishfield et al. (2014) from our simulations of under-ice illuminance. Following recommendations by Reviewer #2, we use the PIOMAS daily data on ice thickness at mooring position from http://psc.apl.uw.edu/research/projects/arctic-sea-ice-volume-anomaly/data/model_grid. New text was introduced in lines 103-111 as follows: "***(ii) For sea-ice thickness, we used grid daily data from the Pan-Arctic Ice Ocean Modeling and Assimilation System (PIOMAS, http://psc.apl.uw.edu/research/projects/arctic-sea-ice-volume-anomaly/data/) developed at the Polar Science Center, University of Washington. PIOMAS is a coupled ocean and sea ice model that assimilates daily sea ice concentration and sea surface temperature satellite products (Zhang and Rothrock, 2003). We used data from the grid node at 71.3°N, 226.7°E closest to the mooring position. Schweiger et al. (2011) reported, that PIOMAS spatial thickness patterns agree well with Ice, Cloud, and land Elevation Satellite (ICESat) thickness estimates (also used in this study) with pattern correlations of above 0.8. However, PIOMAS tends to overestimate thicknesses for the thin ice area around the Beaufort Sea, and underestimate the thick ice area around northern Greenland and the Canadian Archipelago (Wang et al., 2016). The overall differences between PIOMAS and ICESat is -15% or -0.31 m (Wang et al., 2016)"***. Panel b in Figure 3, showing time series of the PIOMAS derived sea-ice thickness, was modified accordingly. We also modified text in lines 167-168, describing sea-ice data used for simulating under-ice illuminance: "*For computing under-ice illumination in Figures* ***3e*** *and* ***3d****,* ***we use daily PIOMAS… data … on the simulated sea-ice thickness…***". As an alternative source of sea-ice thickness data, we used simulations based on the Hybrid Coordinate Ocean Model (HYCOM) + Community Ice Code (CICE) coupled ocean and sea ice system developed at the Danish Meteorological Institute, lines 111-119: "***As an alternative source of sea-ice thickness data, we used (iii) simulations based on the Hybrid Coordinate Ocean Model (HYCOM, v2.2.98; e.g. Chassignet et al., 2007) + Community Ice Code (CICE, v4.0; e.g. Hunke, 2001) coupled ocean and sea ice system, developed at the Danish Meteorological Institute (DMI, Madsen et al., 2016). The horizontal resolution is ~10 km. The model domain covers the Arctic Ocean and the Atlantic Ocean down to ~20°S. Madsen et al. (2016) reported that the simulated sea-ice thickness distribution near the Canadian Arctic Archipelago and the northern coast of Greenland is consistent with CryoSat-2 satellite measurements and the NASA Operation IceBridge airborne observations. Simulated sea-ice thickness, shown in Figure 3b, was derived for the grid node closest to the mooring position. Spatial distributions of sea-ice thickness (Figures 4, 6e, and 6f) were acquired from http://ocean.dmi.dk/arctic/icethickness/thk.uk.php***". Results on illuminance simulations using HYCOM + CICE are presented in new Figure 3e.

3. It is also not clear to me why the authors used two series (Melling et al. 2005 and Krishfield et al. 2014) of the mean seasonal cycle if none of them are from the mooring site and just illustrate typical evolution of sea ice in the region? What's changed if we remove one of them?

Both data sets were eliminated from our analysis. They were replaced with the PIOMAS daily data on ice thickness, as recommended by Reviewer #2, and with the HYCOM + CICE data.

4. I seriously doubt that the presented analysis of the illuminance due to moonlight was carried out convincingly. Figures 6 and 7, where we should see that impact, are very messy and I personally would not say that they show us this relationship in a clear way. For instance, despite the cloudiness during event#6 being about the same low as for events #3 and #4, we do not see any response in MVBS at 28-m depth. Moreover, in Fig. 7 any pattern due to moon phases is not evident at all.

We partly agreed with Reviewer #2. There is no disruption of the DVM signatures in vertical velocity, which can be attributed to the moonlight (Figure 8). We added the corresponding statement in lines 609-610: "***Moreover, under-ice vertical velocity data does not show DVM disruptions during full moon phases (Figure 8)***". We also agree that Figure 7 is messy because the water dynamics and full moon events are often overlaid. For example, the full moon event #6 in February-March 2004, mentioned by Reviewer #2, overlapped with eddy, passing the mooring position from 25 February to 4 March (Figure 10). The uncertain cloud cover also introduces an additional complication. However, there are several full moon events, when the DVM disruptions are obvious. For example, in lines 344-348 we focused on the full moon event #1 in September-October 2004, which clearly shows the downward displacement of the acoustic backscatters in response to the moonlight (Figures 7b, c, g, and f). The full moon event #3 in December 2003 (Figure 7b) also clearly shows the downward displacement of the acoustic backscatters from 24 m (Figure 7c) to 68 m (Figure 7e). We introduced a new piece of text in the beginning of section 6.2, discussing moonlight impact on DVM (lines 604-610): "***In general, interpretation of the DVM modifications due to the moonlight is not straightforward. The dark-time MVBS in Figure 7c shows cumulative effect of sea-ice, cloud cover, water dynamics and moonlight. Individual events are often overlaid, and uncertainty in cloud cover also introduces an additional complication. Furthermore, during February-March, the moonlight below sea-ice is strongly attenuated (2004) or completely absorbed by sea-ice (2005) - Figure 3e. Moreover, under-ice vertical velocity data does not show DVM disruptions during full moon phases (Figure 8)***". We also modified the sentence in lines 615-616 as follows: "***While our results on the moon's modifications of DVM are not entirely conclusive, they are*** *consistent with those previously reported for the Arctic and sub-Arctic regions*". In this context, we also modified our sentence in lines 482-483: "*Our results show that DVM responds to (i) seasonality of the sunlight, (ii) moonlight, and (iii) seasonality of sea-ice cover that attenuates light transmission to the water column****, and to a lesser extent to (iii) moonlight***". Finally, sea-ice thicknesses from HYCOM + CICE helped to reveal that the moonlight during full moon events in February-March 2005 was completely terminated by the ice cover exceeding 2.5 m thick. We added this statement in lines 338-339: "…***3 events in February-March (#7 in 2004 and #6 and 7 in 2005) show complete cessation of the moonlight transmittance through sea-ice exceeding 2.5 m thick (Figure 7b)"*** and lines 327-328: "***Sea-ice strongly attenuates moonlight. Once sea-ice thickness exceeded ~2.5 in April 2004 and February 2005, the moonlight transmittance through sea-ice is completely terminated (Figures 3b and 3e)***".

Specific comments:

5. L61: "228° 38.176'E" Here and throughout the text I suggest using western longitude instead.

Changed as requested, line 66, Figures 1 and 10.

6. L64: "CTD (temperature-salinity-depth)". CTD stands for conductivity-temperature-depth.

Thank you. Corrected in line 69.

7. L71: "…the RDI reports that the vertical velocity is more accurate than the horizontal velocity by at least a factor of two". Could the authors provide a reference for this statement?

Thank you. This reference to RDI is wrong. We improved this statement in lines 75-77 as follows: "*The accuracy of the ADCP vertical velocity measurements is not validated; however,* ***for the 600 kHz RDI***

ADCP, Wood and Gartner (2010) *reported that the vertical velocity is more accurate than the horizontal velocity by at least a factor of two*".

8. L83-87: Please, specify where these data come from and what algorithm was used for ice data processing? I also wonder why the authors used spatially-averaged sea ice concentrations over a 200-km rectangle, not just observations at the site of the mooring. The later looks more logical for the purposes of the assessment of light transmission under specific conditions at the mooring. Could you comment, please?

The data came from https://icdc.cen.uni-hamburg.de/en/seaiceconcentration-asi-amsre.html. They have been computed by applying the ARTIST Sea Ice (ASI) algorithm to brightness temperatures measured with the 89 GHz AMSR-E channels (Spreen et al., 2008). We agree with Reviewer #2 that the sea-ice concentrations derived for the site of the mooring are more appropriate in this context. So, we replaced spatially-averaged sea ice concentrations with those from the pixel closest to the mooring position (see modified Figures 3b, 7a, and 8a). Under-ice illuminance in Figures 7b and 8b was recomputed accordingly. Responding this comment by Reviewer #2, we modified text in lines 91-94 as follows: "***They have been computed by applying the ARTIST Sea Ice (ASI) algorithm to brightness temperatures measured with the 89 GHz AMSR-E channels, and are available through https://icdc.cen.uni-hamburg.de/en/seaiceconcentration-asi-amsre.html. The ASI algorithm is described in Spreen et al. (2008).*** *The spatial grid resolution for ice concentration is 6.25 km,* ***and we used data from the pixel, closest to the mooring position***".

9. L94: ": : :https://rkwok.jpl.nasa.gov/icesat/index.html ". The link provided doesn't exist.

Thank you. Yes, this link certainly disappeared. We modified this sentence in lines 120-122 as follows: "We also used data on sea-ice thickness from ICESat obtained ***from the NASA National Snow and Ice Data Center (Yi and Zwally, 2009)***".

10. L98-100: "Finally, we used (iv) satellite synthetic aperture radar (SAR) imagery acquired by Canadian RADARSAT over the mooring location before the sea-ice breakup in 2004 and 2005 (Figure 5)". Please, provide a source for these images as well.

Responding this comment, we introduced new sentence in lines 127-129 as follows: "***RADARSAT data were acquired through the Government of Canada's Earth Observation Data Management System (https://www.eodms-sgdot.nrcan-rncan.gc.ca***) ".

11. L104-105: "…at times as close as possible to local midnight, with 3 other stations sampled during daytime at times close to midday". Specify the largest time difference between the time of profiling and the local midnight and midday.

This text was omitted following comments #1 by Reviewer #2 and #2 and 6 by Reviewer #1.

12. L127:134: The description of the radiative model is incomplete. It's unclear what was used to calculate illuminance at the top of snow layer. What exactly does the snow thickness series look like? How were ice concentrations and clouds utilized in these calculations? Does this model simulate light distribution in the water layer beneath the sea ice?

This model does not simulate light distribution in the water layer beneath the sea ice. In the original version, we used snow thickness on the top of the ice gradually increasing from zero at freeze-up to a

typical 15-cm thick wind-packed snow in late winter (Melling et al., 2005). In the revised version, however, we derived snow data from AMSR-E/Aqua observations, lines 130-134: "***Snow depth over sea-ice, derived from AMSR-E/Aqua, was obtained from NSIDC (Cavalieri et al., 2014). The 12.5 km snow depth is provided as a 5-day running average. It is generated using the AMSR-E snow-depth-on-sea-ice algorithm based on the spectral gradient ratio of the 18.7 GHz and 36.5 GHz vertical polarization channels (Markus and Cavalieri, 1998). As of the AMSR-E sea-ice concentrations, for generating time series of the snow depth over sea-ice (Figure 3a) we used data from the pixel closest to the mooring position***". We also added this information in lines 169-170: "***The snow thickness on the top of the ice was taken from AMSR-E/Aqua observations***". We added new paned (a) in Figure 3 showing time series of snow thickness on the top of the ice. We also modified text in lines 167-168, describing sea-ice data used for simulating under-ice illuminance: "*For computing under-ice illumination in Figures **3d** and **3e**, **we used PIOMAS and HYCOM+CICE data on the simulated sea-ice thickness, respectively***". We accounted for the sea-ice if its concentration exceeds 90%. We added this statement in lines 170-171: "***We accounted for the sea-ice and snow cover if the sea-ice concentration exceeds 90%***". Finally, we specifically pointed out that the cloud cover data were not used for simulating under-ice illuminance, lines 171-172: "***Cloud cover information is not utilized by this model due to high uncertainty of the cloud cover data (Liu and Key, 2016)"***.

13. L136: "The diurnal signal variation is presented along the vertical axis of the actogram, while the long-term patterns of diurnal behavior…" The meaning is not clear. Did the authors mean variations during a day-long period? What does a "diurnal behavior" mean?

Yes, the "*diurnal behavior*" means variations during a day-long period. We modified this sentence in lines 175-176 as follows: "***Variations during a day-long period are*** *presented along the vertical axis of the actogram*…".

14. L157-159: "Overall, satellite data show that during winter-spring 2005 sea-ice thickness over the mooring location exceeded that for 2004 by >1 m suggesting implications for the under-ice illuminance values". I wonder if this conclusion has any impact on the simulated illuminance.

First, this statement was strengthened involving PIOMAS and HYCOM+CICE data as recommended by Reviewer #2. Second, we compared PIOMAS to HYCOM+CICE and satellite information and revealed that the HYCOM+CICE simulations are better in reproducing sea-ice thickness in winter 2005. This is described in the new paragraph introduced in lines 198-213 alone with impact of the difference between sea-ice thickness in 2004 and 2005 on the simulated illuminance: "***The satellite information on sea-ice thickness, however, is not consistent with PIOMAS. For February-March 2004 and 2005, PIOMAS provides estimates of sea-ice thickness at mooring position of 1.87 m and 2.28 m, respectively (Figure 3b). In contrast, for the same time period, ICESat provides 1.5-1.4 m and 2.4-2.5 m, respectively (Figures 4c and 4d). This discrepancy is in line with the conclusions by Wang et al. (2016) that PIOMAS overestimates thicknesses for the thin ice area around the Beaufort Sea and underestimates the thick ice area around the northern Greenland and the Canadian Arctic Archipelago. For winter-spring 2003-04, PIOMAS data agree relatively well with HYCOM+CICE data (Figure 3b). For January-May 2005, however, the discrepancy between PIOMAS and HYCOM+CICE increases from ~0.5 m on 1 January 2005 to ~1.3 m on 22 May 2005 (Figure 3b). During winter-spring 2005, spatial distribution of sea-ice thickness, derived from HYCOM+CICE simulations, shows the on-slope displacement of the multi-year pack ice from the Greenland and Ellesmere Island shelves (Figure 4), which is also revealed from the***

satellite observations (Figures 5 and 6a-6d). For winter-spring 2005, the HYCOM+CICE data on the multi-year pack ice >2 m thick over the mooring position are in line with detecting multi-year ice on the RADARSAT satellite imagery acquired before sea-ice breakup in May 2005 (Figure 6). *Overall**, the HYCOM+CICE simulations and satellite data suggest show that** during winter-spring 2005 sea-ice thickness over the mooring location exceeded that for 2004 by **~1 m with important implication** for the under-ice illuminance values **as evident from actograms of under-ice illuminance in Figures 3d and 3e. In what follows, we use under-ice illuminance derived using the HYCOM+CICE simulations"***.

15. L161: Likely, the "layer" is missing somewhere.

Fixed in line 215.

16. L194: "…diurnal signal variations". As I noted above, this term is unclear. In actograms presented in Figs. 6-7, changes or variations of diurnal signal are shown along the horizontal axis, not the vertical one. Meanwhile, values along the vertical axis indicate the temporal changes for any specific day, which might be called diurnal cycle or signal, but not its variations. If that is correct, I would suggest the author rephrase this for clarity.

We modified the sentence in lines 248-249 as follows: "*These actograms reveal a rhythm of activity with diurnal **cycle** seen in the vertical axis of an actogram. The 2-year long variability of the diurnal **cycle** is observed along the horizontal axis*".

17. L202-206: Consider merging this paragraph with L45-50 to avoid unnecessary repetition.

Thank you. This text was shortened and moved to lines 54-57: "*Civil twilight is observed at the CA13 latitude from 19 November to 21 January. For the winter solstices (22 December), the civil twilight lasts for about 3 h. The polar day (or the midnight sun, the Sun is above the horizon for the entire 24 hours) lasts at the CA13 latitude from 10 May to 1 August*".

18. L209-210: "Outside of the polar day, the sun illuminance is opposite to MVBS for the sub-surface layer, while at 108 m depth this relationship becomes positive". An awkward sentence because it has meaning only for the diurnal changes, not for the illuminance and MVBS themselves. Please, rephrase.

We modified this sentence in lines 263-264 as follows: "*Outside of the polar day, **the diurnal changes in** the sun illuminance **are** opposite to MVBS for the sub-surface layer, while at 108 m depth this relationship becomes positive*".

19. L211-212: "In spring 2004, the modification of the MVBS diurnal pattern from the beginning of May corresponds to an increase of the midnight under-ice illuminance to >1 lux (Figures 6b and 6c)." I think we need a clarification of what "modification" means here. Is it the vanishing of diurnal pattern? Moreover, I doubt that we can trust this number for the under-ice illuminance if we take into account that sea ice thickness was reproduced by the mean annual cycle.

Yes, we mean the vanishing of diurnal pattern. To clarify this, we slightly modified the sentence in line 265 as follows: "*In spring 2004, the **vanishing** of the MVBS diurnal pattern…*". The under-ice illuminance was recomputed using the PIOMAS and HYCOM+CICE sea-ice thickness (new Figures 3d and 3e, respectively), and snow depth from AMSR-E/Aqua (lines 130-134) following your comments #2 and #12, respectively.

20. L216: According to the description, ICESat data were available only for one spring month (March) in 2004 and 2005. Assuming dynamical nature behind the ice thickness anomaly in 2005, you cannot easily extend this conclusion for the entire spring or specifically to May 2005.

To extend this conclusion for the entire spring 2005, or specifically to May 2005, we used RADARSAT satellite imagery taken before sea-ice breakup on 7 May 2005 (Figures 6c and 6d). This is pointed out in lines 192-197: "*The on-slope displacement of the multi-year pack ice from the Greenland and Ellesmere Island shelves* ***was observed during winter 2005****. This is evident from the sea-ice thickness ICESat data showing a west-southward expansion of the Greenland pack in February - March 2005 (Figure* ***5****d). This is in line with detecting multi-year ice on the RADARSAT satellite imagery acquired over the mooring position* ***in May 2005*** *(Figure* ***6****). The lighter areas in Figures* ***6****c and* ***6****d indicate the multi-year pack ice expanded over the mooring position before the sea-ice breakup in May 2005*". However, this assumption is not consistent with PIOMAS sea-ice thickness data (Figure 3b). The possible explanation is that "…***PIOMAS tends to underestimate the thick ice area around the northern Greenland and the Canadian Arctic Archipelago (Wang et al., 2016)***" – lines 109-110. In our case, for February-March 2004 and 2005, PIOMAS provides estimates of the sea-ice thickness at mooring position of 1.87 m and 2.28 m, respectively (Figure 3b). In contrast, for the same time period, ICESat gives 1.5-1.4 m and 2.4-2.5 m, respectively (Figures 4c and 4d). For justifying our conclusions on sea-ice ice thickness anomaly in 2005, we used HYCOM+CICE simulations (new Figure 4 and new panels e and f in Figure 6), and lines 205-213: "***During winter-spring 2005, spatial distribution of sea-ice thickness, derived from HYCOM+CICE simulations, shows the on-slope displacement of the multi-year pack ice from the Greenland and Ellesmere Island shelves (Figure 4) similar to that revealed from the satellite information (Figures 5 and 6a-6d). For winter-spring 2005, the HYCOM+CICE data on the multi-year pack ice >2 m thick over the mooring position are in line with detecting multi-year ice on the RADARSAT satellite imagery acquired before sea-ice breakup in May 2005 (Figure 6). Overall, the HYCOM+CICE simulations and*** *satellite data* ***suggest*** *that during winter-spring 2005 sea-ice thickness over the mooring location exceeded that for 2004 by* ***~1 m with important implication for the under-ice illuminance values as evident from actograms of under-ice illuminance in Figures 3d and 3e. In what follows, we use under-ice illuminance derived using the HYCOM+CICE simulations***".

21. L216-218: "In spring 2005, the midnight under-ice illuminance >1 lux was lagging that in 2004 by about one week (blue dotted curve in Figure 6b)". What is the reason of this lag if the under-ice illuminance was simulated using the long-term mean seasonal cycle of sea-ice thickness reported by Melling et al. (2005)?

ICESat and RADARSAT data show that during winter 2005 sea-ice was ticker compared to winter 2004 by ~1 m. In the original version of the manuscript, we simulated the difference between winter 2004 and 2005 by artificially increasing the sea-ice thickness since 1 January 2005 by 1 m. In the revised version of the manuscript, we computed the under-ice illuminance using the snow cover and sea-ice thickness provided by the satellite data (Figure 3a) and HYCOM+CICE simulations (Figure 3b), respectively. Newly generated Figures 3e, 7b and 8b show the difference in simulated 1-lux and 0.1-lux thresholds for winters 2004 and 2005. As a result of the thicker ice in April-May 2005, "…*the midnight under-ice illuminance >1 lux was lagging that in 2004 by about one week (Figure* ***7****b)*", lines 271-272.

22. L218-219: "Note that for winter-spring 2005 the under-ice illuminance, shown in colour in Figure 6b, is overestimated by about a factor of 10 (not shown)". I'm very confused by this statement. If this is true, why do the authors show us an incorrect pattern instead of reliable values?

The values of illuminance shown in the original Figures 6b and 7b were obtained based on the seasonal cycle reported by Krishfield et al. (2014) – lines 158-159 in the manuscript original version. The satellite information (both, ICESat and RADARSAT), however, provides an evidence, that the sea-ice thickness in winter 2005 exceeded that for winter 2004 by ~1 m. In the original version of the manuscript, we added this difference to the Krishfield's seasonal cycle since 1 January 2005 to reveal the response of the 1-lux threshold to the ticker ice in 2005. In the revised version, we replaced the Krishfield's seasonal cycle with the PIOMAS and HYCOM+CICE sea-ice thickness as recommended by Reviewer #2. After the PIOMAS data were verified against the satellite data, we chose the HYCOM+CICE simulations. More details explaining this choice are provided in the newly introduced paragraph in lines 198-213. Revised Figures 7b and 8b now show "reliable" values for the under-ice illuminance, which were simulated using HYCOM+CICE data.

23. L223: "diurnal signal was enhanced". What does the enhancement mean in regards to diurnal signal? Is it the increase of diurnal amplitude or what?

Yes, we mean the increase of the MVBS diurnal amplitude. We modified this sentence in lines 277-278 for clarity: "*From **about** 1 April to 10 July 2004, **the diurnal amplitude** of MVBS signal was enhanced at the **6**8-108 m depth layer **due to the MVBS values lowered from ~ -61 to -66 dB** (Figures **7e**-**7**g) **during the astronomic midnight ±3 h***".

24. L224-225: "In contrast to the preceding and subsequent periods, no seasonal tendency in the duration of high/low MVBS was observed at this time." The meaning of this is blurry. Could the author formulate this in a more clear way?

We mean that we did not observe seasonal modulation of the MVBS diurnal cycle. To clarify it, we modified this sentence in lines 278-280 as follows: "*In contrast to the preceding and subsequent periods, **no seasonal modulation of the MVBS diurnal cycle** was observed at this time*".

25. L247: "…with the MVBS diurnal rhythm in Figures 5d-5h." Did the authors mean Fig. 6?

Yes, thank you. Fixed in line 302.

26. L269-270: "During winter, the full moon generates under-ice illuminance up to about 0.1 lux below the sea ice layer with a thickness of around 0.5 m (Figures 3 and 6b)." I cannot understand this. In winter, the sea ice thickness at the mooring site is substantially larger than 1.5 m, not 0.5 m as the authors wrote here. The only months when we see such a thin ice are from July through October, when we see no clear DVM signal.

Thank you. You are totally right. We modified this sentence in lines 324-326 as follows: "*During **mid-**winter **(end of December)**, the full moon generates under-ice illuminance up to about **0.001** lux below the sea**-**ice layer with a thickness of around **1** m **and ~20 cm snow depth over sea-ice** (Figures 3**b** and **7***b)*". We also added two new sentences following this statement (lines 326-328): "***In contrast, for the open water conditions, the full moon generates illuminance exceeding 0.1 lux (Figure 3c). Sea-ice***

strongly attenuates moonlight. Once sea-ice thickness exceeded ~2.5 m in April 2004 and February 2005, the moonlight transmittance through sea-ice is completely terminated (Figures 3b and 3e)".

27. L273-280: I doubt that this result is well justified. Particularly, I didn't see any clear pattern in MVBS shown in Fig. 6c in response to the moonlight variability. It is assumed that we should see similar inclined straps as we see in Fig.6b, but this is not the case. For some periods (e.g., Nov 2003, Feb-March 2004) we didn't see any response in MVBS at all. Thus, I suggest to find another way to present this analysis.

We partly agreed with Reviewer #2. There is no disruption of the DVM signatures in vertical velocity, which can be attributed to the moonlight (Figure 8). We added the corresponding statement in lines 609-610: "***Moreover, under-ice vertical velocity data does not show DVM disruptions during full moon phases (Figure 8)***". We also agree that Figure 7 is messy because the water dynamics and full moon events are often overlaid. For example, the full moon event #6 in February-March 2004, mentioned by Reviewer #2, overlapped with eddy, passing mooring position from 25 February to 4 March (Figure 10). The uncertain cloud cover also introduces an additional complication. However, there are several full moon events, when the DVM disruptions are obvious. For example, in lines 342-347 we focused on the full moon event #1 in September-October 2004, which clearly shows the downward displacement of the acoustic backscatters in response to the moonlight (Figures 7b, c, g, and f). The full moon event #3 in December 2003 (Figure 7b) also clearly shows the downward displacement of the acoustic backscatters from 24 m (Figure 7c) to 68 m (Figure 7e). Responding this comment, we introduced a new text at the beginning of section 6.2, discussing moonlight impact on DVM (lines 606-610): "***In general, interpretation of the DVM modifications due to the moonlight is not straightforward. The dark-time MVBS in Figure 7c shows cumulative effect of sea-ice, cloud cover, water dynamics and moonlight. Individual events are often overlaid, and uncertainty in cloud cover also introduces an additional complication. Furthermore, during February-March, the moonlight below sea-ice is strongly attenuated (2004) or completely absorbed by sea-ice (2005) - Figure 3e. Moreover, under-ice vertical velocity data does not show DVM disruptions during full moon phases (Figure 8)***". We also modified the sentence in lines 615-616 as follows: "***While our results on the moon's modifications of DVM are not entirely conclusive, they are*** *consistent with those previously reported for the Arctic and sub-Arctic regions*". In this context, we also modified our sentence in lines 482-483: "*Our results show that DVM responds to (i) seasonality of the sunlight, (ii) moonlight, and (iii) seasonality of sea-ice cover that attenuates light transmission to the water column****, and to a lesser extent to (iii) moonlight***". Finally, sea-ice thicknesses from HYCOM + CICE helped to reveal that the moonlight during full moon events in February-March 2005 was completely terminated by the ice cover exceeding 2.5 m thick. We added this statement in lines 338-339: "…***3 events in February-March (#7 in 2004 and #6 and 7 in 2005) show complete cessation of the moonlight transmittance through sea-ice exceeding 2.5 m thick (Figure 7b)"*** and lines 327-328: "***Sea-ice strongly attenuates moonlight. Once sea-ice thickness exceeded ~2.5 m in April 2004 and February 2005, the moonlight transmittance through sea-ice is completely terminated (Figures 3b and 3e)***".

28. L298-299: "These deviations, however, can also be attributed to inclinations of the ADCP transducer due to high-velocity currents." Note, that ADCP automatically corrects that inclinations. The reason might be just more dynamical (turbulent) state of the environment associated with larger currents.

Thank you. Responding this comment, we introduced a new paragraph in lines 355-363 as follows: "***The vertical velocity component is very sensitive to spatial inhomogeneity of the flow field and errors in the ADCP tilt angle, introducing errors and significant contamination to the measured vertical velocity component (Ott, 2005). This is consistent with contamination of the vertical velocity data observed during upwellings, downwellings and eddy passing (Figures 8c-8g). Deviations of vertical velocity diurnal pattern can also be attributed to more dynamical (turbulent) state of the environment associated with high-velocity currents.*** *In what follows, we are only interested in the vertical velocity estimates, which are sensitive to the MVBS diurnal cycling.* ***The contaminated vertical velocity data cannot be used for interpretation DVM modifications imposed by upwellings, downwellings, and eddies. Therefore, our analysis on impact of the major energetic events on DVM is entirely based on vertical redistribution of the acoustic backscatters (Figures 7c-7g, 9a and 9b)***".

29. L331-332: "moving MVBS upwards." Please, rephrase because MVBS cannot move anywhere.

Thank you. We changed this sentence in lines 402-403 as follows: "*Downwelling events disrupt the MVBS diurnal signal in the opposite way compared to upwellings and moonlight, moving* ***acoustic backscatters*** *upwards*".

30. L337: "It seems that downwelling #3D is entirely dominated by the moon…" Do the authors claim that the Moon impacts downwelling somehow?

We do not claim this, of course. We modify this sentence in line 409 for clarity: "*It seems that* ***event*** *#3D is entirely dominated by the moon…*".

31. L376-377: "It appears that this MVBS anomaly is attributed to the eddy-entrained suspended particles commonly recorded in this area (O'Brien et al., 2011)." If the disruptions of diurnal cycle are attributed to higher concentration of suspended materials in the eddy, why do we see such an unusual pattern in vertical velocity around the core in Fig. 7? I mean very high positive anomalies of the vertical velocity during the day time at 68- and 88-m depths. And a more general question: the authors noted in Discussion that "zooplankton likely avoids enhanced water dynamics" (L539). In that regards, why we do not see vertical migration of both signs in layers above and below the eddy core where we have the strongest currents?

For the first part of this comment, please see our response to your comment #37, and text newly introduced in lines 355-363. Responding the second part of this comment, we clarify that below the eddy core the DVM signal was inverted (lines 444-445). Above the eddy, MVBS is slightly elevated during the light time (Figures 7c, 7g and 10c). The possible interpretation is that zooplankton partially occupied the sub-surface layer during the light time avoiding enhanced water dynamics attributed to eddy passing. To present our results on eddy impact on DVM in a more clear way, we modified our sentence in lines 445-446 as follows: "*At 28-48 m depth, however, MVBS was not* ***significantly*** *modified.* ***Nevertheless, MVBS was slightly elevated during the light time (Figures 7c, 7g and 10c)***".

32. L378: "December/January 2002/2003 ". Check the period.

Changed to "***2003/2004***" in lines 450 and 456, thank you.

33. L403-404: "Our results show that DVM responds to (i) seasonality of the sunlight, (ii) moonlight, and (iii) seasonality of sea-ice cover that attenuates light transmission to the water column." I intuitively

agree with that statement, but I should emphasize that the authors partially fail to demonstrate DVM associated with sea ice changes and moonlight variations. See my other comments.

Please see our responses to your comments #2, 4, 12, 14, 20, 21, 22, 27, 28, and 34.

34. L445-446: "The inter-annual variability in estimated under-ice illuminance is entirely attributed to the sea-ice thickness." How was this conclusion made if the mean annual cycle for sea ice thickness was used to simulate the under-ice illuminance? In Fig. 3, for example, I see no difference in ice draft among 2003/04 and 2004/05.

Following general comment #2 by Reviewer #2, we completely removed a mean seasonal cycle of ice thickness by Melling et al. (2005) and Krishfield et al. (2014) from our simulations of under ice illuminance. Following the recommendations provided by Reviewer #2, we use PIOMAS and HYCOM + CICE simulated sea-ice thickness data derived for the mooring position. Panel b in Figure 3 now shows PIOMAS-and HYCOM + CICE derived sea-ice thickness data used for computing under-ice illumination in Figures 3d and 3e, respectively. Figures 7b and 8b were recomputed for HYCOM + CICE data on sea-ice thickness.

35. L446-448: "During the ice season, the mean cloud cover (~40%) showed insignificant interannual variability (Figure 6a); thus, the cloud cover was not taken into account." This, again, raises the question about what was included in the model to simulate light illuminance.

Description of the model to simulate light illuminance in lines 161-172 was improved following comment #12 by Reviewer #2. We specifically make note that "***Cloud cover information was not utilized by this model due to high uncertainty of the cloud cover data (Liu and Key, 2016)***", lines 171-172.

36. L550-551: "It appears that upwelling, downwelling, and eddies disrupt DVM by generating a water layer with an enhanced gradient of horizontal velocity." Could the author explain how "the wind-driven barotropic flow generated by upwelling and downwelling wind forcing" (L543) can enhance velocity gradients? If barotropic means depth-uniform current, it cannot produce vertical gradients. Or do the authors mean lateral gradients?

The wind-driven barotropic flow generated by upwelling and downwelling is superimposed on the background bottom-intensified shelfbreak current. For downwelling, this flow amplifies the depth-intensified background baroclinic circulation with enhanced Pacific water transport towards the Canadian Arctic Archipelago. For upwelling, the shelfbreak current is reversed, which results in surface-intensified flow in the opposite direction (Dmitrenko et al., 2018). This is schematically depicted in Figure 11c and explained in figure caption in lines 1041-1044: *"(c) Schematic depiction suggesting generation of the surface-intensified (blue curve) and depth-intensified (red curve) along-slope currents as a result of upwelling and downwelling, respectively, superimposed on the hypothetical bottom-intensified shelfbreak current (black dashed curve) following Dmitrenko et al. (2018)*". The impact of velocity lateral gradients (cross-slope transport), comprised of upwelling and downwelling, is discussed in lines 634-641: "*The characteristic feature of high-energetic events recorded at CA13 is the depth-dependent behavior of the horizontal flow. For upwelling and downwelling over the eastern Beaufort Sea continental slope, this feature is generated by the superposition of the background and wind-forced flow (Dmitrenko et al., 2018). The wind-driven barotropic flow generated by upwelling and downwelling wind forcing is superimposed on the background bottom-intensified shelfbreak current depicted by a dashed*

line in Figure 11c (Dmitrenko et al., 2018). For the downwelling storms, this effect amplifies the depth-intensified background circulation with enhanced PWW transport towards the Canadian Arctic Archipelago (Figure 11b and 11c, right). For the upwelling storms, the shelfbreak current is reversed, which results in surface-intensified flow moving in the opposite direction (Dmitrenko et al., 2018 and Figures 11a and 11c, left)". The impact of along-slope transport, comprised by upwelling and downwelling, is discussed below in lines 662-665: "*We speculate that DVM disruptions attributed to upwelling and downwelling are primarily dominated by along-slope transport rather than the cross-slope transport. In addition to enhancing the cross-slope transport, upwelling and downwelling over the Beaufort Sea continental slope strongly modify along-slope transport through generating depth-dependent currents over the continental slope (Figure 11; Dmitrenko et al., 2016, 2018)*".

37. L594 and Fig. 7: This paragraph is confusing. Why do the events of upwelling and downwelling (e.g., 9U and 10D, and many others) have the same positive sign for the vertical velocity within the entire water layer? If we assume that the response of zooplankton to those events is to avoid layers with enhanced water dynamics (l.601), we should see the opposite direction in zooplankton migration in the case of bottom-intensified downwelling and surface-intensified upwelling. However, following Fig.7, this is not the case. Keeping in mind my previous comment to L376-377, I would say that the presented materials on vertical velocities do not support the author's conclusion at all.

We disagree with this comment by Reviewer #2. During the upwelling and downwelling events, the vertical velocity is very noisy (Figures 8c-8g). The vertical velocity component is much more sensitive than the horizontal component to biases inherent in the measurement process itself, such as spatial inhomogeneity of the flow field and errors in the ADCP tilt angle, owing to the fact that the vertical velocity component is typically an order of magnitude smaller – Ott (2005, doi: 10.1016/j.csr.2004.09.007). Ott (2005) also pointed out that the spatial inhomogeneity of the flow can introduce errors in the measured vertical velocity component. Small errors in the measured pitch, roll and tilt can also lead to significant contamination of the vertical velocity. This is consistent with contamination of the vertical velocity observed during high energetic events at CA13 such as upwellings, downwellings and eddy passing. Thus, vertical velocity cannot be used for interpretation of DVM modifications imposed by upwellings, downwellings, and eddies. Therefore, we build our conclusions based on vertical redistribution of the acoustic backscatter (Figures 7c-7g, 9a and 9b). To clarify our approach, we introduced a new paragraph in lines 355-363 as follows: "***The vertical velocity component is very sensitive to spatial inhomogeneity of the flow field and errors in the ADCP tilt angle, introducing errors and significant contamination to the measured vertical velocity component (Ott, 2005). This is consistent with contamination of the vertical velocity data observed during upwellings, downwellings and eddy passing (Figures 8c-8g). Deviations of the vertical velocity diurnal pattern can also be attributed to a more dynamical (turbulent) state of the environment associated with high-velocity currents.*** *In what follows, we are only interested in the vertical velocity estimates, which are sensitive to the MVBS diurnal cycling.* ***The contaminated vertical velocity data cannot be used for interpretation of DVM modifications imposed by upwellings, downwellings, and eddies. Therefore, our analysis on impact of the major energetic events on DVM is entirely based on vertical redistribution of the acoustic backscatters (Figures 7c-7g, 9a and 9b)***".

38. L604-611. Please, see my general comment regarding the analysis of zooplankton.

Following comments #1 by Reviewer #2 and #2 and 6 by Reviewer #1, this section was omitted.

39. L621-622: “The ADCP data are available through the Polar Data Catalogue at https://www.polardata.ca/pdcsearch/, CCIN Reference #11653 (Gratton et al., unpublished).” This dataset is not available using the CCIN Reference provided.

The ADCP data are available using this CCIN Reference number. Please click on DATA/MAP:

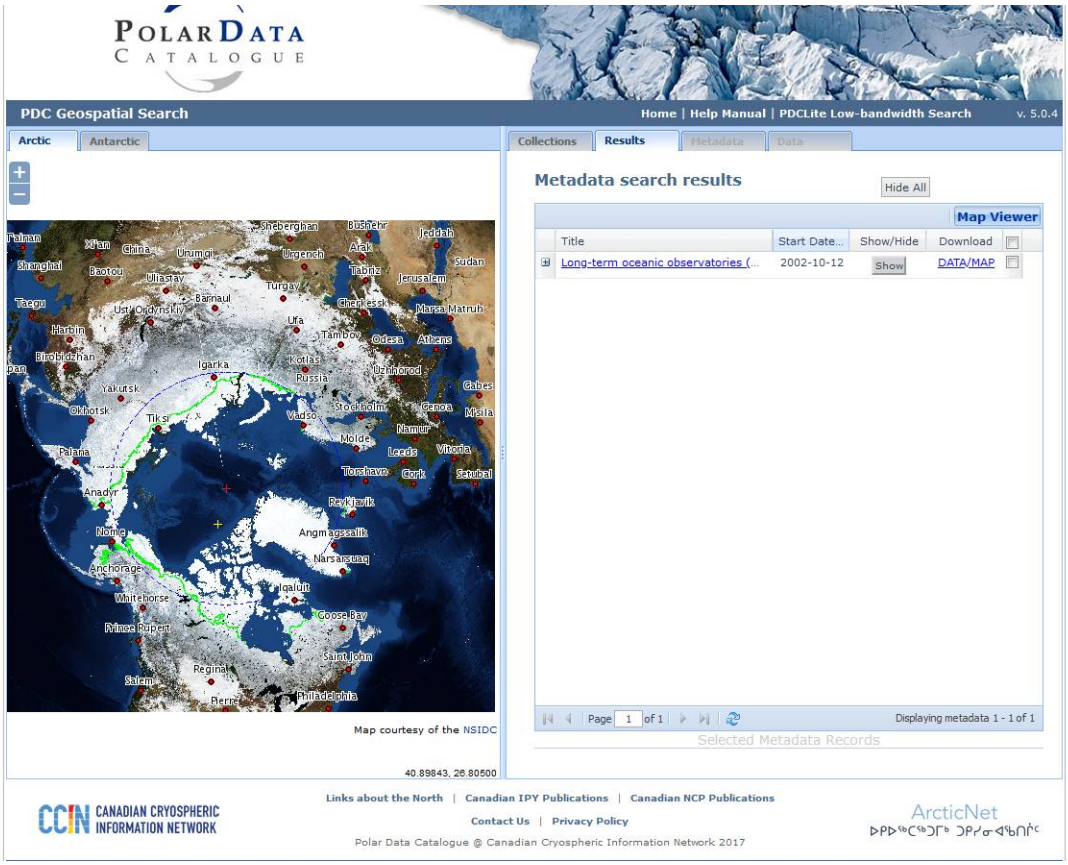

This will lead you to the data sets:

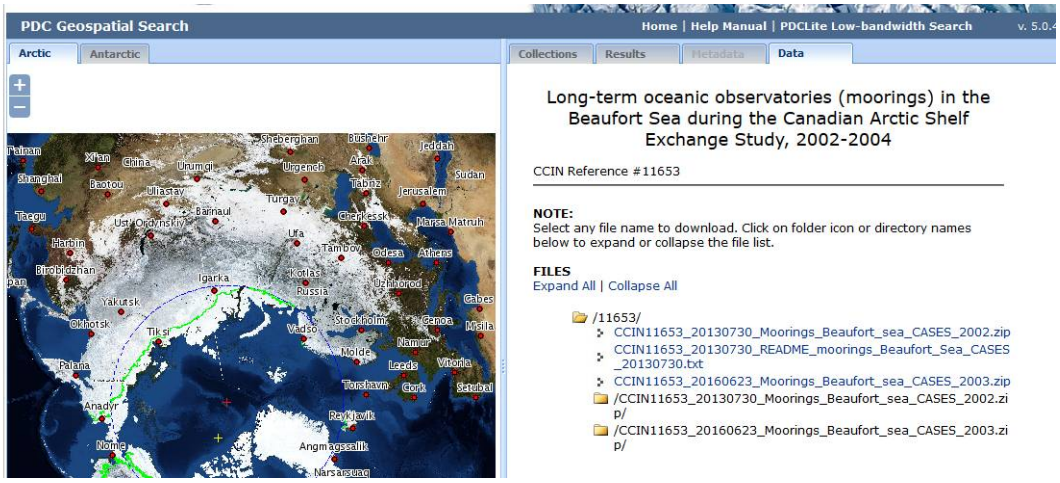

40. Figure 7: I would suggest the author use a different color scheme for this figure to separate positive and negative vertical velocities in a clearer way. For example, using a white color at zero velocity may help.

We tried different color codes for this figure (Figure 8 in the revised version). However, the light green was found to produce the best possible artificial visual boundary to red and blue, depicting the upward and downward movements, respectively.

Sea-ice and water dynamics and moonlight impact the acoustic backscatter diurnal signal over the eastern Beaufort Sea continental slope

Igor A. Dmitrenko[1], Vladislav Petrusevich[1], Gérald Darnis[2], Sergei A. Kirillov[1], Alexander S. Komarov[3], Jens K. Ehn[1], Alexandre Forest[2], Louis Fortier[2], Søren Rysgaard[1,4] and David G. Barber[1]

[1]Centre for Earth Observation Science, University of Manitoba, Winnipeg, R3T 2N2, Canada
[2]Department of Biology, Laval University, Québec City, G1V 0A6, Canada
[3]Data Assimilation and Satellite Meteorology Research Section, Environment and Climate Change Canada, Ottawa, K1G 3Z4, Canada
[4]Arctic Research Centre, Aarhus University, Aarhus, DK-8000, Denmark

Correspondence to: Igor A. Dmitrenko (igor.dmitrenko@umanitoba.ca)

Abstract. A two-year-long time series of currents and acoustic backscatter from an Acoustic Doppler Current Profiler, moored over the eastern Beaufort Sea continental slope from October 2003 to September 2005, were used to assess dynamics and variability of the sound-scattering layer. It has been shown that acoustic backscatter is dominated by a synchronized diel vertical migration (DVM) of the zooplankton. Our results show that DVM timings (i) were synchronous with sunlight, and (ii) were modified by moonlight and sea-ice, which attenuates light transmission to the water column. Moreover, DVM is modified or completely disrupted during highly energetic current events. Thicker ice observed during winter-spring ~~2004~~ 2005 lowered the backscatter values, but favored extending DVM toward the midnight sun. In contrast to many previous studies, DVM occurred through the intermediate water layer during the ice-free season of the midnight sun in 2004. In 2005, the midnight sun DVM was likely impacted~~masked~~ by a high acoustic scattering generated by suspended particles. During full moon at low cloud cover, the nighttime moonlight illuminance led to zooplankton avoidance of the sub-surface layer disrupting DVM. Moreover, DVM was disrupted by upwelling, downwelling and eddy passing. We suggest that these deviations are consistent with DVM adjusting to avoid enhanced water dynamics. For upwelling and downwelling, zooplankton likely respond to the along-slope water dynamics dominated by surface- and depth-intensified flow, respectively. This drives zooplankton to adjust DVM by aggregating in the low or upper intermediate water layer for upwelling and downwelling, respectively. The baroclinic eddy reversed DVM below the eddy core.

1 Introduction

The acoustic backscatter signal recorded in the ocean by acoustic Doppler current profilers (ADCPs) is mainly dominated by zooplankton. The diurnal patterns of the acoustic backscatter signal are comprised of diel vertical migration (DVM) of zooplankton, the synchronized movement of zooplankton up and down in the water column over a daily cycle (e.g., Brierley,

2014). In terms of biomass, DVM is arguably the largest daily migration of animals on earth (Hays, 2003), and the largest non-human migration (Brierley et al., 2014). DVM has been extensively explored in the Arctic using either echo sounders or zooplankton nets (e.g., Kosobokova, 1978; Fortier, et al., 2001; Blachowiak-Samolyk et al., 2006; Cottier et al., 2006; Falk-Petersen et al., 2008). The latest progress in assessing DVM in the Arctic is related to understanding DVM during the Arctic polar night (Berge et al., 2009, 2015) and the role of moonlight in modifying DVM (Last et al., 2016; Petrusevich et al., 2016). While significant progress has been achieved in understanding DVM, the sea-ice and ocean dynamics control on DVM in the Arctic environment remains poorly appreciated.

ADCPs moored over the entire annual cycle in the seasonally ice-covered Arctic water provide a unique temporal evolution of the DVM patterns. This seasonal perspective is essential to achieve a more complete and quantitative understanding of DVM in response to the light and sea-ice conditions (e.g., Tran et al., 2016; Hobbs et al., 2018). Here we assess temporal evolution of the DVM patterns using a two-year-long time series of velocity and acoustic backscatter from an ADCP-equipped mooring deployed over the upper eastern Beaufort Sea continental slope from October 2003 to September 2005 (Figure 1). The ADCP limitation, however, comes from its ability to detect only the biomass moving at a population level, i.e., comprising the migrating sound-scattering layer (Hobbs et al., 2018). ~~We partly overcame this disadvantage by using zooplankton samples collected in September 2016 in the southeastern Beaufort Sea (Figure 1a).~~

The oceanographic ~~environmental~~ factors controlling DVM in the seasonally ice-covered Arctic areas, located at the inner border of the polar circle, remains poorly assessed. Here we use observations from the oceanographic mooring located at ~71°N, the area, where the Sun is between 0 and <6° below the horizon all day on the winter solstice. At t~~T~~his latitude no actual daylight is experienced during short winter daylight hours with the exception of ~~corresponds to the~~ civil twilight ~~Polar twilight~~ when solar illumination is still sufficient for the human eye to distinguish terrestrial objects. ~~during short winter daylight hours~~. This geographical position makes our DVM observational site vastly different from those at Svalbard (astronomical twilight, the Sun is between 12 and 18° below the horizon~~nautical polar night~~, ~80°N; e.g., Grenvald et al., 2016; Darnis et al., 2017), Canada Basin (nautical twilight, the Sun is between 6 and 12° below the horizon~~civil polar night~~, ~77.5°N; La et al., 2018), and Northeast Greenland (nautical twilight~~civil polar night~~, ~74.5°N, Petrusevich et al., 2016). Civil twilight is observed at the CA13 latitude from 19 November to 21 January. For the winter solstices (22 December), the civil twilight lasts for about 3 h. The polar day (or the midnight sun, the Sun is above the horizon for the entire 24 hours) lasts at the CA13 latitude from 10 May to 1 August.

This study is built on results by Dmitrenko et al. (2018) on water dynamics over the eastern Beaufort Sea continental slope taking advantage of using the ADCP-derived acoustic backscatter for temporal appreciation of DVM patterns during two consecutive annual cycles. Our particular focus is on the DVM modifications, caused by wind-forced upwelling and downwelling over the Beaufort Sea continental slope, and the different types of sea-ice cover. We also add more data points and further proof to research focused on the effect of moonlight on DVM (e.g., Webster et al., 2015; Last et al., 2016; Petrusevich et al., 2016).

2 Data

We used data from the ArcticNet oceanographic mooring CA13 deployed over the upper Canadian Beaufort Sea continental slope at 300-m depth from 9 October 2003 to 4 September 2005 at 71°21.356'N, 131~~228~~°21~~38~~.~~176~~824'~~E~~W (Figure 1). The mooring description can be found in Dmitrenko et al. (2016). For this study, we used (i) velocity and acoustic backscatter intensity records from a 300 kHz upward-looking Workhorse Sentinel ADCP by Teledyne RD Instruments (RDI) at 119-m depth and (ii) temperature records from the moored CTD (conductivity-temperature~~-salinity~~-depth) SBE-37 by Sea-Bird Electronics, Inc. at 49-m and 119-m depth. The velocity and acoustic backscatter data were obtained at 8-m depth intervals, with a 1-h ensemble time interval and 30 pings per ensemble. The first bin was located at ~9 m above the transducer, i.e., at 108 m depth. For this research, we used bins at 28, 68, and 108 m depth. Data at 48 and 88 m depth were obtained by linear interpolation between bins at 44 m and 52 m, and 84 m and 92 m, respectively. The RDI ADCP precision and resolution are ± 0.5% and ± 0.1 cm s^{-1}, respectively. The standard deviation for an ensemble average of 30 pings for the 8-m depth cell size is reported by RDI to be 1.19 cm s^{-1}. The accuracy of the ADCP vertical velocity measurements is not validated; however, for the 600 kHz RDI ADCP, Wood and Gartner (2010) ~~the RDI~~ reported~~s~~ that the vertical velocity is more accurate than the horizontal velocity by at least a factor of two. The compass accuracy is ± 2°. The magnetic deviation was added. The along-slope direction was determined to be 64°T (°T - the direction measured with reference to the true north) using the scatterplot of the daily mean velocity data following an assumption that the maximum dispersion of velocity measurements occurs along the continental slope (Dmitrenko et al., 2016). Mooring data were complemented by the vertical CTD, chlorophyll fluorescence and particulate beam attenuation profiles taken at mooring deployment and recovery in October 2003 and September 2005, respectively, and in July 2004 using a CTD probe SBE-911 (Figure 2). According to the manufacturers' estimates, individual temperature and conductivity measurements are accurate to ±0.001°C and ±0.0003 S m^{-1}, respectively, for the SBE-911, and to ±0.002°C and ±0.0003 S m^{-1} for SBE-37.

The total cloud cover (%) for the mooring location is obtained from the National Centers for Environmental Prediction - NCEP (Kalnay et al., 1996). The accuracy of the cloud cover data is uncertain. Comparing the satellite- to NCEP-derived cloud cover over the Arctic (60°-90°N) for 2000-2014 shows that NCEP data underestimates the mean cloud cover amount by about 25-30% all year round (Liu and Key, 2016).

For sea-ice, we use the following five~~four~~ different data sets. (i) Sea-ice concentrations (Figure 3b) are derived from the Advanced Microwave Scanning Radiometer for EOS (AMSR-E) with errors less than 10% for ice concentrations above 65% (Spreen et al., 2008). They have been computed by applying the ARTIST Sea Ice (ASI) algorithm to brightness temperatures measured with the 89 GHz AMSR-E channels and are available through https://icdc.cen.uni-hamburg.de/en/seaiceconcentration-asi-amsre.html. The ASI algorithm is described in Spreen et al. (2008). The spatial grid resolution for ice concentration is 6.25 km, and we used data from the pixel, closest to the mooring position. ~~. The time series of sea-ice concentration was obtained by averaging the daily data at all grid nodes over the eastern Beaufort Sea area limited by 220°E to 230°E and 70°N to 72°N. (ii) The long-term mean annual cycles of the first- and multi-year pack ice draft were~~

adapted from Melling et al. (2005) and Krishfield et al. (2014), respectively (Figure 3). Melling et al. (2005) compiled the mean annual cycle in the sea ice draft of the first year pack ice using data from the Ice Profiling Doppler Sonar (IPS) by ASL Environmental Sciences deployed over the eastern Beaufort Sea shelf between 1991 and 2003 at about 50 m depth, 156 km southwestward from the CA13 mooring. Krishfield et al. (2014) computed the mean annual cycle in the multi year pack ice draft using the IPS data from the Canada Basin. We used their data from the IPS at mooring BGOS-D (74°N, 220°E) deployed from 2006 to 2012 about 400 km northwestward from the CA13 mooring.

For sea ice thickness, we used (ii) grid daily data from the Pan-Arctic Ice Ocean Modeling and Assimilation System (PIOMAS, http://psc.apl.uw.edu/research/projects/arctic-sea-ice-volume-anomaly/data/) developed at the Polar Science Center, University of Washington. PIOMAS is a coupled ocean and sea ice model that assimilates daily sea-ice concentration and sea surface temperature satellite products (Zhang and Rothrock, 2003). We used data from the grid node at 71.3°N, 133.3°W closest to the mooring position. Schweiger et al. (2011) reported, that PIOMAS spatial thickness patterns agree well with Ice, Cloud, and land Elevation Satellite (ICESat) thickness estimates (also used in this study) with pattern correlations of above 0.8. However, PIOMAS tends to overestimate thicknesses for the thin ice area around the Beaufort Sea, and underestimate the thick ice area around northern Greenland and the Canadian Arctic Archipelago (Wang et al., 2016). The overall differences between PIOMAS and ICESat is -15% or -0.31 m (Wang et al., 2016). As an alternative source of sea-ice thickness data, we used (iii) simulations based on the Hybrid Coordinate Ocean Model (HYCOM, v2.2.98; e.g. Chassignet et al., 2007) + Community Ice Code (CICE, v4.0; e.g. Hunke, 2001) coupled ocean and sea ice system, developed at the Danish Meteorological Institute (DMI, Madsen et al., 2016). The horizontal resolution is ~10 km. The model domain covers the Arctic Ocean and the Atlantic Ocean down to ~20°S. Madsen et al. (2016) reported that the simulated sea-ice thickness distribution near the Canadian Arctic Archipelago and the northern coast of Greenland is consistent with CryoSat-2 satellite measurements and the NASA Operation IceBridge airborne observations. Simulated sea-ice thicknesses, shown in Figure 3b, were derived for the grid node closest to the mooring position. Spatial distributions of sea-ice thickness (Figures 4, 6e, and 6f) were acquired from http://ocean.dmi.dk/arctic/icethickness/thk.uk.php.

(iv) We also used data on sea-ice thickness from the Ice, Cloud, and land Elevation Satellite (ICESat) obtained from through https://rkwok.jpl.nasa.gov/icesat/index.html the NASA National Snow and Ice Data Center – NSIDS (Yi and Zwally, 2009)(Figure 4). Data represent the gridded 25-km means. Kwok et al. (2007) found a mean uncertainty of the sea-ice thickness of about 0.7 m, and the sea-ice draft estimated from ICESat data relative to that measured at moorings agreed within 0.5 m. We use data from the ICESat campaigns previously used by Kwok et al. (2009): ON03 (24 September - 18 November 2003), FM04 (17 February – 23 March 2004), ON04 (3 October – 8 November 2004), and FM05 (17 February – 24 March 2005) shown in Figure 54. Finally, we used (iv) satellite synthetic aperture radar (SAR) imagery acquired by Canadian RADARSAT over the mooring location before the sea-ice breakup in 2004 and 2005 (Figures 6a-6d5). RADARSAT data were acquired through the Government of Canada's Earth Observation Data Management System (https://www.eodms-sgdot.nrcan-rncan.gc.ca).

Snow depth over sea-ice, derived from AMSR-E/Aqua, was obtained from NSIDC (Cavalieri et al., 2014). The 12.5 km snow depth is provided as a 5-day running average. It is generated using the AMSR-E snow-depth-on-sea-ice algorithm based on the spectral gradient ratio of the 18.7 GHz and 36.5 GHz vertical polarization channels (Markus and Cavalieri, 1998). As of the AMSR-E sea-ice concentrations, for generating time series of the snow depth over sea-ice (Figure 3a) we used data from the pixel closest to the mooring position.

~~Zooplankton samples were collected in September 2016 at six stations in the southeastern Beaufort Sea (Figure 1a) from the CCGS *Amundsen*. The positions of the stations are the following: St. 405: 70.606°N, 236.964°E, st. 435: 71.074°N, 226.356°E, st. 406 69.972°N, 237.039°E, st. 437: 71.801°N, 233.501°E, st. 403: 70.100°N, 239.893°E, st. 575: 76.181°N, 234.041°E. To identify the taxa involved in DVM, we compared 3 stations sampled during nighttime, at times as close as possible to local midnight, with 3 other stations sampled during daytime at times close to midday. A double square net, fitted with two 1 m^2 aperture nets (mesh size 500 and 750 µm), was obliquely deployed at a maximum sampling depth of about 90 m and at a ship speed of two knots. The duration of the plankton net tow varied between 4.5 and 9.8 min. Flowmeters at the mouth of each net were used to calculate the volume of water filtered during net deployment. Upon recovery, fish larvae were rapidly sorted out of the samples. Then, the sample from the 500 µm mesh net was preserved in a borax buffered seawater solution of 4% formaldehyde for taxonomic identification. In the laboratory, each sample was sieved through a 1000-µm sieve to retain the zooplankton to be identified. The sample was transferred into a large transparent dish from which all the macrozooplankton organisms (mainly, jellyfish, large chaetognaths, amphipods and euphausiids) were sorted, counted and identified to species level. Known volume aliquots containing approximately 300 organisms were taken from the remainder of the sample using a Motoda splitting box and the zooplankton were counted and identified to the lowest taxonomic level possible.~~

3 Methods

We analyzed the acoustic backscatter and velocity time series from ADCP to reveal modifications of the acoustic backscatter diurnal signal primarily dominated by DVM. In general, the particles in the water column producing a significant portion of acoustic backscatter comprise suspended sediments or planktonic organisms (e.g., Petrusevich et al., 2020). Frazil ice crystals also generate an enhanced acoustic backscatter (e.g., Dmitrenko et al., 2010). However, sound scattering produced by zooplankton is more complex compared to that generated by sediment particles due to DVM (Stanton et al., 1994). Moreover, ADCPs, unlike echo-sounders, are limited in deriving accurate quantitative estimates of zooplankton biomass (Lemon et al., 2001, 2012; Vestheim et al., 2014). This is mainly due to calibration issues (Brierley et al., 1998; Fielding et al., 2004; Lemon et al., 2008; Lorke et al., 2004) and the beam geometry (Vestheim et al., 2014). To account for the beam geometry, we derived mean volume backscatter strength (MVBS) in dB from the acoustic backscatter echo intensity following the procedure described by Deines (1999).

Under-ice illumination ~~(Figures 6b and 7b)~~ was modelled using the exponential decay radiative transfer model (Grenfell and Maykut, 1977; Perovich, 1996). Figure 3c shows the sea-surface illuminance at mooring position computed for

the open water conditions (no sea-ice and snow cover). Transmittance through the sea ice and snow cover to depth z in the ice was calculated using the following equation: $T(z) = i_0 e^{-K_t z}$, where i_0 is the fraction of the wavelength-integrated incident irradiance transmitted through the top 0.1 m of the surface layer, and K_t is the total extinction coefficient in the snow or sea ice cover. The values adopted for the sea ice and snow covers were i_0=0.63, K_t=1.5, and i_0=50.9, K_t=0.1, respectively (Grenfell and Maykut, 1977). For computing under-ice illumination in Figures 3d~~6b~~ and 3e~~7b~~, we use PIOMAS and HYCOM+CICE data on the simulated sea-ice thickness, respectively~~the mean (2006-2012) annual cycle derived from the IPS data by Krishfield et al. (2014) – Figure 3~~. The snow thickness on the top of the ice was taken from AMSR-E/Aqua observations~~gradually increasing from zero at freeze-up to a typical 15-cm thick wind-packed snow in late winter (Melling et al., 2005).~~ We accounted for the sea-ice and snow cover if the sea-ice concentration exceeds 90%. Cloud cover information was not utilized by this model taking due to high uncertainty of the cloud cover data (Liu and Key, 2016).

Time series of MVBS (Figures ~~6~~7c-7g), vertical velocity component (Figures 8~~7~~c-8g) and surface layer illumination (Figures 7~~6~~b and 8~~7~~b), computed for the HYCOM+CICE sea-ice thickness, are presented in a form of actograms showing a rhythm of activity. Variations during a day-long period ~~The diurnal signal variation is~~are presented along the vertical axis of the actogram, while the long-term patterns of diurnal behavior can be assessed following the horizontal axis (e. g., Leise et al., 2013; Last et al., 2016; Hobbs et al., 2018). For the actograms of illuminance~~In Figures 6b and 7b~~ we introduced an artificial visual boundary on the illuminance colour scheme at 1 lux (gray to orange), the threshold, which corresponds to illuminance during the deep twilight.

Following Barber et al. (2015), we used the kinetic energy, $E = (U^2 + V^2) / 2$, derived from the zonal (U) and meridional (V) components of the current velocity to identify the major energetic events exceeding the two standard deviation threshold of ~ 500 cm^2 s^{-2}. Using this threshold, Dmitrenko et al. (2018) identified thirteen major energetic events comprised of upwellings and downwellings. They are highlighted in Figures 7~~6~~-9~~8~~ with blue and pink shadings, respectively.

4 Sea-Ice and Oceanographic Settings

4.1 Sea-ice

The southern Beaufort Sea is seasonally ice-covered. It is dominated by the first-year pack ice with thickness gradually increasing from zero in September to ~80-90 cm in March-April (Melling et al., 2005)~~ – Figure 3~~. In the Canada Basin beyond the eastern Beaufort Sea continental slope, ice conditions are partly dominated by the multi-year pack ice with a mean thickness increasing from about 30 cm in August-September to 210-220 cm in May (Krishfield et al., 2014)~~ – Figure 3~~. The multi-year Greenland pack ice (>7 m thick) occupies the area to the north of the Canadian Arctic Archipelago and Greenland (e.g., Kwok et al., 2009).

~~During winter 2005~~, T~~t~~he on-slope displacement of the multi-year pack ice from the Greenland and Ellesmere Island shelves was observed during winter 2005~~disrupted the long-term mean seasonal cycle~~. This is evident from the sea-ice thickness ICESat data showing a west-southward expansion of the Greenland pack in February - March 2005 (Figure 5~~4~~d).

This is in line with detecting multi-year ice on the RADARSAT satellite imagery acquired over the mooring position in May 2005 (Figure 6~~5~~). The lighter areas in Figures 6~~5~~c and 6~~5~~d indicate the multi-year pack ice expanded over the mooring position before the sea-ice breakup in May 2005.

The satellite information on sea-ice thickness, however, is not consistent with PIOMAS. For February-March 2004 and 2005, PIOMAS provides estimates of sea-ice thickness at mooring position of 1.87 m and 2.28 m, respectively (Figure 3b). In contrast, for the same time period, ICESat provides 1.5-1.4 m and 2.4-2.5 m, respectively (Figures 4c and 4d). This discrepancy is in line with the conclusions by Wang et al. (2016) that PIOMAS overestimates thicknesses for the thin ice area around the Beaufort Sea and underestimates the thick ice area around the northern Greenland and the Canadian Arctic Archipelago. For winter-spring 2003-04, PIOMAS data agree relatively well with HYCOM+CICE data (Figure 3b). For January-May 2005, however, the discrepancy between PIOMAS and HYCOM+CICE increases from ~0.5 m on 1 January 2005 to ~1.3 m on 22 May 2005 (Figure 3b). During winter-spring 2005, spatial distribution of sea-ice thickness, derived from HYCOM+CICE simulations, shows the on-slope displacement of the multi-year pack ice from the Greenland and Ellesmere Island shelves (Figure 4), which is also revealed from the satellite observations (Figures 5 and 6a-6d). For winter-spring 2005, the HYCOM+CICE data on the multi-year pack ice >2 m thick over the mooring position are in line with detecting multi-year ice on the RADARSAT satellite imagery acquired before sea-ice breakup in May 2005 (Figure 6). Overall, the HYCOM+CICE simulations and satellite data suggest ~~show~~ that during winter-spring 2005 sea-ice thickness over the mooring location exceeded that for 2004 by ~~~~>~~1 m with important implication ~~suggesting implications~~ for the under-ice illuminance values as evident from actograms of under-ice illuminance in Figures 3d and 3e. In what follows, we use under-ice illuminance derived using the HYCOM+CICE simulations.

4.2 Temperature and salinity

The structure of the near-surface and intermediate water layers over the eastern Beaufort Sea upper continental slope, resolved by ADCP, is comprised of a mixture of river runoff and sea-ice meltwater and seawater of Pacific origin (Figure 2). A surface layer of relatively warm and low-salinity water (~27-29) is freshened by the Mackenzie River runoff and sea-ice melt. Water with the salinity $29 < S < 33$ is generally assigned to Pacific Water (PW) – e.g., Dmitrenko et al. (2016). It is transported along the Beaufort Sea continental slope by an Alaskan branch of the PW flow emanating from Bering Strait. The relatively fresh PW layer impacts the halocline structure, producing a double halocline layer with a low stratified Upper Halocline water formed by the insertion of PW that overlies Lower Halocline water originating from the Eurasian Basin. In this study, we associated PW with the broad temperature range between 1.5°C and –1.5°C approximately centered at $S \sim 32$ residing upper and low halocline layers (Figure 2). Pacific Summer Water (PSW) is broadly classified here as $T > –1.2$°C and $30 < S < 32$ (pink shading in Figure 2). In October 2003, July 2004, and September 2005, PSW occupied the upper intermediate water layer from ~25 to ~60 m depth (Figure 2). This water mass is usually comprised of the Chukchi Summer water transported through Herald Canyon on the western Chukchi shelf (Woodgate et al., 2005) and the Alaskan Coastal water transported by the Alaskan coastal current through Barrow Canyon (Pickart et al., 2005). The underlying Pacific Winter Water (PWW) with

the broad temperature minimum below –1.2°C centred at S ~ 33 (blue shading in Figure 2) is generated during freezing and brine rejection in the Bering and Chukchi Seas (Weingartner et al., 1998; Pickart, 2004). During 2003-2005, PWW occupied the lower intermediate water layer in ~60-140 m depth (Figure 2). The warm and saltier Atlantic water with temperatures above 0°C and S > 33.5 underlies PWW at depths > 230 m that significantly exceeds the depth range resolved with ADCP measurements (Figure 2).

4.3 Water dynamics

The kinetic energy of currents over the eastern Beaufort Sea continental slope is mainly affected by the along-slope current component (Kulikov et al., 1998; Williams et al., 2006; Dmitrenko et al., 2016, 2018). For CA13, the maximum variability of currents is also consistent with along-slope direction, explaining ~ 70% of the total velocity variability (Dmitrenko et al., 2018). Thus, major energetic events highlighted in Figures 7-9~~6-8~~ are primarily associated with along-slope flow dynamics, as also follows from the velocity time series in Figures ~~8~~9c and ~~8~~9d. Among thirteen major energetic events in Figures 7-9~~6-8~~, four events were clearly attributed to the depth-intensified flow (#3D, 4D, 6D and 10D; pink shading in Figures 7-9~~6-8~~) generated by ocean downwelling superimposed on the background bottom-intensified eastward shelfbreak flow. Six events are associated with the surface-intensified or barotropic flow (#1U, 2U, 7U, 8U, 9U, and 12U; blue shading in Figures 7-9~~6-8~~). These events were attributed to ocean upwelling (Dmitrenko et al., 2018). While events #5U and 11U are depth-intensified, they are highlighted with blue shading because they are consistent with upwelling-favorable atmospheric forcing that usually drives the surface-intensified events. Vice versa, event #13D is surface-intensified, but it has been highlighted with pink shading because it is consistent with downwelling-favorable atmospheric forcing (Dmitrenko et al., 2018).

5 Diurnal Signal of the Mean Volume Backscatter Strength (MVBS) and Vertical Velocity

MVBS and vertical velocity actograms were computed for the depth of 28, 48, 68, 88 and 108 m (Figures 7~~6~~c-7g and 8~~7~~c-8g). These actograms reveal a rhythm of activity with diurnal cycle ~~signal variations~~ seen in the vertical axis of an actogram. The 2-year long variability of the diurnal cycle~~pattern~~ is observed along the horizontal axis.

5.1 Seasonal patterns

In general, MVBS actograms resemble seasonal variability of the diurnal signal following light conditions (Figures 7~~6~~b-7g and 8~~7~~b-8g). In the subsurface layer (28 m depth), a low MVBS corresponds to a relatively high illuminance during the day, while an elevated MVBS is consistent with a low illuminance during the night (Figures 7~~6~~b and 7~~6~~c). In contrast, at 108 m depth, MVBS shows an opposite pattern with a high MVBS during the light time of the day and a low MVBS in the darkness (Figures 7~~6~~b and ~~6~~7g). This variability in MVBS is consistent with DVM.

~~The main factor controlling surface and under-ice illuminance is solar altitude. Civil polar night (the sun is between 6° and 12° below the horizon for the entire 24 hours) does not occur for CA13 at ~71.3°N. Civil twilight (the sun is down to 6° below the horizon) is observed at the CA13 latitude from 18 November to 21 January (Figures 6b and 7b). For the winter~~

~~solstices (22 December), the civil twilight lasts for about 3 h. The polar day (midnight sun) occurs when the sun is above the horizon for the entire 24 hours. At the CA13 latitude, the polar day lasts 82 days from 10 May to 31 July.~~

In general, the MVBS diurnal signal follows the seasonal variability of the sun illuminance during the entire year except for the period of the polar day when the diurnal pattern becomes significantly disrupted in the sub-surface water layer. Outside of the polar day, the diurnal changes in the sun illuminance are~~is~~ opposite to MVBS for the sub-surface layer, while at 108 m depth this relationship becomes positive. During the polar day, in the subsurface layer the MVBS diurnal rhythm vanishes (Figure 7~~6~~c). In spring 2004, the vanishing ~~modification~~ of the MVBS diurnal pattern from the beginning of May corresponds to an increase of the midnight under-ice illuminance to >0.1 lux (Figures ~~6~~7b and ~~6~~7c). This modification lagged behind the sea-ice retreat off the mooring location by about one month (Figures 7~~6~~a and 7~~6~~c). In contrast, during spring 2005, significant deviation of the MVBS diurnal rhythm was delayed by about 3 weeks compared to 2004. The deviation of the MVBS diurnal pattern was recorded once the sea-ice disappeared from the mooring location on 20 May 2005. Note that the satellite-derived data and HYCOM+CICE simulations for winter-spring 2005 show the sea-ice thickness over the mooring location exceeding that for 2004 by ~~>~~1 m (Figures 4-~~6 and 5~~). In spring 2005, the midnight under-ice illuminance >1 lux was lagging that in 2004 by about one week (~~blue dotted curve in~~ Figure ~~6~~7b). ~~Note that for winter-spring 2005 the under-ice illuminance, shown in colour in Figure 6b, is overestimated by about a factor of 10 (not shown). Note that the under-ice illuminance has been simulated using the long-term mean seasonal cycle of sea-ice thickness reported by Melling et al. (2005). The ICESat data set has no capacity for generating the sea-ice thickness seasonal cycle for 2003-2005.~~

For the PW layer, the behavior of the MVBS diurnal signal during the polar day is different from the sub-surface water layer. From about 1 April to 10 July 2004, the diurnal amplitude of MVBS ~~diurnal~~ signal was enhanced at the ~~6~~48-108 m depth layer due to MVBS values lowered from ~ -61 to -66 dB during the astronomic midnight ±3 h (Figures 7~~6~~c~~d~~-7~~6~~g). In contrast to the preceding and subsequent periods, no seasonal modulation of the MVBS diurnal cycle ~~tendency in the duration of high/low MVBS~~ was observed at this time. This is in line with illuminance, showing almost no seasonal modulation during the midnight sun (Figure 7~~6~~b). For the polar day period in 2005, however, enhancement of the MVBS diurnal signal seemed to be ~~masked~~impacted by the short-term high MVBS events likely generated by intrusions of turbid water. These events were found to be most pronounced through the PSW layer where intrusions of turbid and relatively warmer water were observed during mooring recovery (Figures 2c, ~~6~~7d, and 7~~6~~e).

Following the midnight sun, the MVBS diurnal signal returned once the mooring position becomes 100% ice-covered since 7 November 2003 and 25 October 2004 (Figures ~~6~~7a and 7~~6~~c-7~~6~~g). This is evident from enhancing the MVBS difference between the light (> 1 lux) and dark (< 1 lux) time for 28-48 m depth (Figure 7~~6~~c-7~~6~~d). The noticeable feature of the MVBS diurnal signal during civil twilight and the subsequent period until the end of April is a significant MVBS difference between 2003-2004 and 2004-2005 observed during the dark time through the entire water column resolved with ADCP observations (Figures 7~~6~~c-7~~6~~f). Another noticeable feature of MVBS during this period is numerous disruptions of the diurnal signal discussed below in sections ~~3.2.2~~5.3.1 and ~~3.2.3~~5.3.2.

Behind seasonality of diurnal signal in the MVBS time series, the seasonal cycling of the MVBS vertical distribution has been revealed (Figures 9~~8~~a and 9~~8~~b). For midnight, during low-light conditions from October to February (civil twilight length exceeds daylight length), MVBS tends to increase with depths from 28 to 108 m depth (Figure 8a). In March-June, the midnight MVBS shows an opposite tendency (Figure 9~~8~~a). The MVBS midnight long-term mean, however, shows almost no difference from 28 to 108 m depth with a long-term mean of -0.6 dB. The seasonal cycle of the MVBS vertical distribution for the astronomic noon is different. From about winter to summer solstices, MVBS at 128 m depth exceeds that for 28 m depth by about 8 dB (Figure 9~~8~~b). In contrast, during the ice-free period in June-August, the MVBS difference from 28 to 108 m depth tends to decrease down to about zero in late summer. The long-term mean for the astronomic noon (-5.3 dB, Figure 9~~8~~b) shows a general tendency of MVBS to increase with depth.

The vertical velocity actograms also show a diurnal pattern around astronomic midnight (Figures 8~~7~~c-~~7~~8g) that is consistent with the MVBS diurnal rhythm in Figures 7~~5~~d-7~~5~~h. Net upward movement is regularly observed before the astronomic midnight once the under-ice dark-time illuminance was <0.1 lux (Figures ~~7~~8b-8~~7~~g). Moreover, the most intense upward flow was recorded during 1-3 h after the illuminance dropped below the 0.1 lux threshold. In contrast, a downward net flow was recorded following the tendency of under-ice illuminance to increase from midnight to noon once illuminance exceeds the 0.1 lux threshold (Figures 8~~7~~b-8~~7~~g). At the end of April 2004, once under-ice illuminance exceeded the 0.1 lux threshold for 24 h a day approaching the midnight sun, the vertical velocity diurnal signal completely vanished. During May-June 2004, however, a weaker net upward and downward diurnal movement of about ±0.5 cm s^{-1} was recorded at 68 and 88 m depth from noon to midnight (light blue to green shading in Figures 8~~7~~e and 8~~7~~f), and from midnight to noon (light green to yellow shading in Figures 8~~7~~e and 8~~7~~f), respectively. This is consistent with the MVBS diurnal rhythm revealed through the PW layer during summer 2004 (Figures 7~~6~~e-~~6~~7g). Following the under-ice illuminance, well-pronounced velocity diurnal signal again appeared since end of ~~mid-~~August 2004 when the midnight under-ice illuminance decreases to the 0.1 lux threshold gradually returning to civil twilight. In spring 2005, the vertical velocity diurnal signal was relatively well pronounced until the midnight under-ice illuminance is below the 0.1 lux threshold (Figures 8~~7~~b-8~~7~~g). As of MVBS, complete cessation of a diurnal signal in vertical velocity in spring 2005 was observed at 68-88 m depth only when sea-ice started to retreat in mid-May (Figure ~~7~~8a). In this case, complete cessation of diurnal signal lagged the 0.1 lux threshold by about 2~~1~~0 days (Figures 8~~7~~b, 8~~7~~e, and 8~~7~~f). During the midnight sun 2005, the velocity diurnal rhythm is unrecognizable.

Finally, the velocity diurnal signal varies with depth. The upward and downward flow attributed to diurnal cycling is higher and less noisy at 68-88 m depth compared to the overlaying sub-surface layer at 28-48 m depth and to a lesser extent to the underlying water at 108 m depth (Figures 8~~7~~c-~~7~~8g).

5.2 Moon cycle

During the period of civil twilight when the sun is more than 6° below the horizon, the moonlight was the main source of illumination over the eastern Beaufort Sea continental slope (Figure ~~6~~7b). The full moon succeeds with a mean period of 29.53059 days called a synodic or lunar month. During mid-winter (end of December), the full moon generates under-ice

illuminance up to about 0.001 lux below the sea-ice layer with a thickness of around 0.51 m and ~20 cm snow depth over sea-ice (Figures 3b and 7b). In contrast, for the open water conditions, the full moon generates illuminance exceeding 0.1 lux (Figure 3c). Sea-ice strongly attenuates moonlight. Once sea-ice thickness exceeded ~2.5 m in April 2004 and February 2005, the moonlight transmittance through sea-ice is completely terminated (Figures 3b and 3e). While the cloud cover attenuates moon illumination, it was not considered for modelling under-ice illuminance due to high uncertainty of the cloud cover data (Liu and Key, 2016).

The MVBS diurnal signal is impacted by the moonlight, also attenuated by the cloud cover. Once the full moon (±6 days) occurred during the period of civil twilight, the cloud cover shows three low-cloud events with cloud cover ≤ 30% (#3, 4 in 2003-2004 and #3 in 2004-2005 in Figures 7a and 7b). During these events, the MVBS diurnal signal was significantly disrupted in the sub-surface layer, and a low MVBS was observed during the entire 24 h (Figures 7bc and 7c). For the full moon event #4 in January 2004, during the astronomic midnight, a low MVBS at 28 m depth was associated with an elevated MVBS at 108 m depth, as evident from decreasing the MVBS difference from 28 to 108 m depth in Figure 8a. Overall, among 14 full moon events occurred in October-March 2003-2004 and 2004-2005 once the midnight under-ice illuminance was <1 lux, 3 events in February-March (#7 in 2004 and #6 and 7 in 2005) show complete cessation of the moonlight transmittance through sea-ice exceeding 2.5 m thick (Figure 7b). 10 Eevents #1-5 in 2003-2004 and #1, 2, and 5 in 2004-2005 demonstrated similar, but less intense anomalies of the MVBS difference from 28 to 108 m depth (events #1-3, 4,5, and 7 in 2003-2004 and #1, 2, 5 and 7 in 2004-2005, (Figure 9a). During the noon, however, this pattern is not obvious (Figure 8b).

Full moon event #1 in September-October 2004 gives an example of the moonlight impact on the MVBS diurnal signal (Figure 7). While the cloud cover during this event was relatively high (~50%, Figure 7a), the dark-time MVBS dropped by ~2 dB at 28 m depth, but elevated by ~4 dB at 68 and 88 m depth suggesting the downward displacement of the acoustic backscatters (Figures 7c and 7f-7g, respectively). At noon, however, MVBS elevated by ~4 dB at 28 m depth (Figure 7c). Note that during this time the under-ice illuminance reduced as the mooring became ice-covered (Figure 7a). It is also important to point out that this full moon event partly overlays with upwelling #7U described below.

5.3 Short-term oceanographic events

The regular diurnal pattern of MVBS was disrupted during the short-term events lasting from several days to several weeks (Figures 7d-7h). These events also interplay with disruptions generated by moon cycling. We use actograms of vertical velocity to differentiate disruptions imposed by moonlight from those of dynamic origin (Figures 8c-8g). In general, the diurnal pattern remains well recognizable during the full moon events (Figures 8b-8g). In contrast, almost all significant or even complete short-term disruptions of the vertical velocity diurnal rhythm are related to upwelling or downwelling (Figures 8c-8g).

The vertical velocity component is very sensitive to spatial inhomogeneity of the flow field and errors in the ADCP tilt angle, introducing errors and significant contamination to the measured vertical velocity component (Ott, 2005). This is consistent with contamination of the vertical velocity data observed during upwellings, downwellings and eddy passing

(Figures 8c-8g). Deviations of the vertical velocity diurnal pattern can also be attributed to a more dynamical (turbulent) state of the environment associated with high-velocity currents. In what follows, we are only interested in the vertical velocity estimates, which are sensitive to the MVBS diurnal cycling. The contaminated vertical velocity data cannot be used for interpretation of DVM modifications imposed by upwellings, downwellings, and eddies. Therefore, our analysis on impact of the major energetic events on DVM is entirely based on vertical redistribution of the acoustic backscatters (Figures 7c-7g, 9a and 9b).

Dmitrenko et al. (2018) identified upwelling or downwelling events at CA13 using ADCP velocity data, the NCEP-derived wind and sea-level atmospheric data, sea surface height records at Tuktoyaktuk (Figure 1) and numerical simulations. All these events are highlighted in Figures 7-9~~5 7~~ with blue and red shadings for upwelling and downwelling, respectively. ~~Vertical displacement of water parcel attributed to upwelling or downwelling generates a noise of vertical velocity deviating its diurnal pattern. These deviations, however, can also be attributed to inclinations of the ADCP transducer due to high-velocity currents. In the following, we are only interested in the vertical velocity estimates, which are sensitive to the MVBS diurnal cycling.~~

5.3.1 Upwelling Events

Upwelling events disrupt the MVBS diurnal signal in a similar way as the moonlight does. For upwelling #1U, MVBS at 108 m depth was elevated throughout the full 24 h period (Figure ~~6~~7g). During the dark time (illuminance < 1 lux) at 28 m depth, MVBS reduced to the end of the event when the surface-intensified flow at 28 m depth shows maximum velocities exceeding 30 cm s^{-1} (Figure 9~~8~~c). Moreover, upwelling #1U resulted in ~0.7°C temperature increase at 119 m depth (Figure 9~~8~~f). Upwelling #2U, occurred right before the winter solstice, shows significant MVBS reduction at 28-48 m depth gradually vanishing to 108 m depth. Upwelling #5U occurred at the end of the ice-free season and shortly after the end of the midnight sun 2004. Therefore, the MVBS diurnal signal was relatively weak and noisy, especially at 28 m depth. However, MVBS increase at 88-108 m depth is likely attributed to upwelling. Upwelling #7U interplayed with full moon event #1 in September-October 2004. It seems that the first portion of this event until 3 October 2004 was dominated by the moonlight. Afterward, once the horizontal velocity at 28 m depth exceeded ~30 cm s^{-1} (Figure 9~~8~~c), a slight reduction of MVBS is observed in 28-48 m depth during the dark time. In contrast to the preceding upwelling events, no elevated MVBS values were recorded in the overlying water layer. Upwelling #8U completely coincided with full moon event #2 in October-November 2004. As with the majority of the full moon and upwelling events, it shows the downward redistribution of the acoustic backscatters from 28-48 m to the deeper water layer (Figures 7~~6~~c-7~~6~~g, 9~~8~~a, and 9~~8~~b). A similar overlap between full moon and upwelling was observed during upwelling #9U. Significant MVBS reduction within 28-48 m was accompanied by elevated MVBS in 88-108 m depth during the latter part of this upwelling from 25 November to 5 December 2004. Overall, upwelling events #7-9 resulted in a gradual increase of temperature at 119 m depth from -1.55°C to -0.65°C (Figure 9~~8~~f). Upwelling #11U shows an elevated MVBS during the light time at 88-108 m (Figures 7~~6~~f, 7~~6~~g, and 9~~8~~b). However, no significant modifications of the MVBS diurnal signal were observed in the overlying water. The last upwelling #12U in May-June 2005 occurred during the midnight

sun when the MVBS diurnal signal mostly vanished, and MVBS is noisy. We speculate that this noise is due to the enhanced concentration of suspended particles in the water column (Figure 2c).

Overall, among 8 upwelling events observed in 2003-2005, 6 events (#1, 2, 5, 7, 8, 9U) clearly show the MVBS reduction in the subsurface water layer at 28 m depth (Figure 76c). For upwellings #1, 5, 7, and 8U the midnight MVBS difference from 28 to 108 m depth tends to decrease, which is consistent with a downward redistribution of acoustic scatters (Figure 98a). This effect is similar to the MVBS response to the full moon events as described in section 5.2. It seems that the overlay between the upwelling and full moon can dominate the MVBS response to upwellings #7-9U (Figures 76b-76g). During the polar day, the MVBS diurnal signal is weak or completely disrupted, and its response to upwelling is barely traceable (upwelling #12, Figure 76b-76g). Finally, wind, forcing upwelling events, also impacts the sea-ice cover through the off-shelf displacement of the pack ice as evident for upwelling event #12 in May-June 2005 (Figure 7a).

5.3.2 Downwelling Events

Downwelling events disrupt the MVBS diurnal signal in the opposite way compared to upwellings and moonlight, moving acoustic backscattersMVBS upwards. Downwelling also interferes with MVBS modifications imposed by sea-ice and the MVBS diurnal signal deviations generated by moonlight. Wind, forcing downwelling events, also impacts the sea-ice cover through the on-shelf displacement of the pack ice as evident for downwelling events #4, 6 and 13D (Figure 76a). Deviations of the MVBS diurnal signal due to moon cycling interferes with those caused by downwelling event #3 complicating our analysis.

Downwelling #3D occurred at the end of 2003-2004 during civil twilight and strongly interfered with full moon event #4 (Figure 76). It seems that eventdownwelling #3D is entirely dominated by the moon, disrupting the MVBS diurnal signal as described in section 5.2. Downwelling #4D was recorded at the end of the polar day 2004 when the MVBS diurnal signal is terminated at 28-88 m depth (Figures 76c-76f). Wind, forcing downwelling #4D, displaced pack ice on-shelf, and the CA13 position was reoccupied by sea-ice for about 10 days with implication for under-ice illuminance. Figures 76c and 76d show that sea-ice and downwelling did not impact MVBS at 28-48 m depth. In contrast, the midnight sun diurnal signal at 68-88 m depth was disrupted due to elevating MVBS at 68-88 m depth during the dark-time (from 22 to 4 h, Figures 76e and 76f). At the same time, the midnight sun diurnal signal at 108 m depth remained undisturbed (Figure 76g). Downwelling #6D provides the most comprehensive example of how the MVBS diurnal signal is disrupted by downwelling. In contrast to the full moon and upwelling events, MVBS at 28-48 m depth was enhanced 24 h a day (Figures 76c and 76d) suggesting the upward redistribution of the acoustic backscatters from the underlying water layer (Figures 89a and 98b). Note that during this event water dynamics was dominated by along-slope depth-intensified flow increasing from ~5 cm s^{-1} at 28 m depth (Figure 98c) to >30 cm s^{-1} at 108 m depth (Figure 98d). Downwelling #10D was recorded at the end of civil twilight 2004-2005. It appears that the beginning of this event is impacted by the full moon (#4, 2004-2005) with the reduction of MVBS in the sub-surface layer at 28 m depth. However, by the end of downwelling #10D, once the bottom-intensified flow exceeded 100 cm s^{-1} at 128 m (Figure 98d), MVBS at 28-48 m depth tended to increase suggesting the upward redistribution of the acoustic backscatters,

similar to downwelling #6D. Downwelling #13D occurred in mid-August 2005 following the midnight sun. During this time, the MVBS diurnal signal at 28 depth was not traceable. At 48-88 m depth, the midnight sun diurnal signal was likely masked due to the enhanced concentration of suspended particles in the water column (Figure 2c).

Overall, among 5 downwelling events recorded in 2003-2005, event #6D and partly #10D show disruption of the MVBS diurnal signal in the sub-surface water layer with MVBS elevated at 28-48 m depth in response to downwelling. Downwelling events #4 and 13D occurred during and shortly after the midnight sun, respectively, when the sub-surface MVBS diurnal signal vanishes. Downwelling event #3D was dominated by the moonlight.

5.3.3 Eddies

Eddies are ubiquitous over the Arctic Ocean continental slope (e.g., Dmitrenko et al., 2008; Pnyushkov et al., 2018), and particularly over the Beaufort Sea continental slope (e.g., Spall et al., 2008; O'Brien et al., 2011). The eddy carrying entrained suspended particles was identified by Dmitrenko et al. (2018) based on the ADCP velocity and acoustic backscatter time series in February–March 2004 (Figures 7~~6~~ and 10~~9~~). One more eddy passed mooring position in December/January 2003/2004 right before downwelling #3D. In Figures 6-8 both eddies are highlighted with yellow shading.

The eddy in February–March 2004 provides an example of how the velocity field attributed to eddy passing disrupts the MVBS diurnal signal (Figure 10~~9~~). The greatest tangential speed, exceeding 22 cm s^{-1}, marks the eddy core near 95 m depth (Figures 10~~9~~a and 10~~9~~b). Below the core at 119 m depth, a positive temperature anomaly of 0.25°C attributed to the eddy passing was recorded on 26 February 2004 (Figure 9~~8~~f). The velocity signature of the eddy is hardly discernible shallower than about 50 m, where the temperature anomaly does not exceed ~0.1°C (Figures 9~~8~~e, ~~9~~10a, and 10~~9~~b). During the dark time at 108 m depth (below the depth of the greatest tangential speed), an enhanced MVBS was observed between two maximal of the eddy tangential speed from 27 February to 2 March 2004 (Figure 10~~9~~d). In contrast, during the daylight, a negative MVBS anomaly was recorded (Figures 7~~6~~g and 10~~9~~d). This completely inverted the MVBS diurnal signal observed at 108 m depth during the eddy passing. At 28-48 m depth, however, MVBS was not significantly modified. Nevertheless, MVBS was slightly elevated during the light time (Figures 7c, 7g and 10c). ~~(Figure 9c).~~ In contrast to water layers above and below the eddy core, from 26 February to 1 March the MVBS diurnal signal at 68-88 m depth was disrupted by the backscatter maximum recorded for 24 h a day (Figures 7~~6~~e and 7~~6~~f). It appears that this MVBS anomaly is attributed to the eddy-entrained suspended particles commonly recorded in this area (O'Brien et al., 2011).

The eddy in December/January ~~2002/2003~~2003/2004 generated much less MVBS disturbance compared to the one in February–March 2004 (Figures 7~~6~~c-7~~6~~g). The core of the eddy was likely deeper than the ADCP transducer. A positive temperature anomaly at 119 m depth was 0.5°C (Figure 9~~8~~f). A positive MVBS anomaly was recorded only at 108 m depth during 24 h a day (Figure 7~~6~~g) likely indicating the eddy-entrained suspended particles. MVBS in the overlaying water layer was not significantly modified.

In summary, the eddy in February–March 2004 inverted the MVBS diurnal signal in the water layer below the eddy core defined by the greatest tangential speed of the horizontal flow. The eddy in December/January 20032/20043 generated no significant MVBS modifications as the eddy core was likely located below the ADCP.

6 Zooplankton

The assemblage of organisms making the large mesozooplankton size class (>1 mm) was more abundant at night (34–65 ind. m^{-3}) than in the day (4–12 ind m^{-3}) within the top 90 m of the water column. This difference in zooplankton's total abundance between day and night was mainly due to the higher abundance of the large copepods *Calanus glacialis* and *Metridia longa* at night (Figure 10a).

The abundance of the macrozooplankton size class was much lower than that of the large mesozooplankton, representing between 0.3% and 8% of the total zooplankton assemblage. However, the difference of total macrozooplankton abundance between night and day was not as clear as for the large mesozooplankton size class. No species stood out as being more abundant at night than at day (Figure 10b).

67 Discussion

The two-year-long ADCP time series of MVBS and vertical velocity over the upper eastern Beaufort Sea continental slope are consistent with DVM of zooplankton. MVBS diurnal signal is generated by a diurnal movement of zooplankton toward the surface at dusk, and descent back the next morning before dawn. DVM demonstrates predator-avoidance behavior (Hays, 2003). Zooplankton keeps away from a relatively well-illuminated surface water layer during the light time reducing the light-dependent mortality risk. The acoustic data from the single-frequency ADCP do not provide any information on the identity of organisms responsible for the observed DVM patterns, and proper studies on DVM have not been carried out in the Beaufort Sea prior to the present work. Thus, our analysis is significantly limited by deficiency of zooplankton observations. Moreover, a comprehensive analysis of the scattering species comprising DVM is logistically impossible for the long-term deployments in the seasonally ice-covered and remote areas in the high Arctic. This prohibits identification of specific species whose DVM was detected by the 300 kHz ADCP and altered by the different environmental factors including illuminance and water dynamics. The deficiency of our analysis clearly defines a necessity for expanding mooring observations using underwater electronic holographic cameras such as those described by Sun et al. (2007).

In general, DVM at CA13 is controlled by light conditions (Figures 76 and 87). As for the other areas of the ocean, DVM is triggered by local solar variations, and the timing of migration is sensitive to changes in seasonal day length (e.g., van Haren and Compton, 2013). Our results show that DVM responds to (i) seasonality of the sunlight, (ii) moonlight, and (iii) seasonality of sea-ice cover that attenuates light transmission to the water column, and to a lesser extent to (iii) moonlight. Moreover, (iv) DVM can be modified or completely disrupted during highly energetic current events generated by upwelling, downwelling or eddy passing. Our results also suggest that the interplay between all these factors impacts DVM at CA13. Furthermore, MVBS is not entirely controlled by DVM. The suspended particles in the water column enhance acoustic

scattering, impactingmasking DVM during the midnight sun (Figures 2a, and 76b, 76d, and 76e), and also attenuating light intensity in the water column. Below we discuss all these factors and their impact on DVM in more detail.

7.1 Zooplankton species generating DVM

The acoustic data from the single-frequency ADCP do not provide any information on the identity of organisms responsible for the observed DVM patterns, and proper studies on DVM have not been carried out in the Beaufort Sea prior to the present work. Differences in the zooplankton composition and abundances at night and in the day, revealed by plankton net sampling in the surface layer of sampling stations around the location of the mooring, indicate that the large copepods *Calanus glacialis* and *Metridia longa* were performing DVM in September. Their density in the surface layer was higher at night than at day in September 2016. The advanced developmental stages (copepodites CIV-adults) of these species have also been found to perform DVM in the other parts of the Arctic, such as Barrow Strait in the central Canadian Arctic Archipelago in May and June (Fortier et al., 2001), and around the Svalbard Archipelago in the European Arctic in September (Daase et al., 2008). Among the large copepods in the Svalbard Kongsfjord, only *M. longa* performed DVM in February at the termination of the polar night (Grenvald et al., 2016). *Calanus glacialis* and *M. longa* CIV-adults are >2.2 mm in length, providing them with good backscatter potential at the 300 kHz frequency of the ADCP (Berge et al., 2014). Thus, they were likely detected by the ADCP and contributed to the diel signals recorded.

Grenvald et al. (2016) also found that the euphausiids *Thysanoessa* spp. had the highest backscatter potential in February in Kongsfjord, partly due to their large macrozooplankton size, and were most likely responsible for the DVM patterns observed at that time. Although, *Thysanoessa* spp. were found in our zooplankton samples, their abundance, or that of any other euphausiids, was very low in September 2016 at the six sampling stations considered in our study. In fact, the lack of convincing day-night difference in the abundances of any of the taxa belonging to the macrozooplankton size class is not necessarily indicative of an absence of DVM behaviour on their part. Our sampling method, mostly designed to capture small fish larvae, may just have not been efficient enough for quantitative sampling of fast swimming macrozooplankton crustaceans such as pelagic amphipods and euphausiids, known to perform DVM in other regions. Furthermore, comparison of day and night plankton net samples from different locations may introduce variability, which is difficult to characterize due to a limited number of stations used in our study. A more thorough approach to properly identify the zooplankton species engaged in DVM should rely on much larger plankton nets, and day-night sampling events at the same locations over several stations to account for spatial difference and patchiness. This would represent a significant logistical challenge in the remote Arctic marine systems. Moreover, the deficiency of our analysis clearly defines a necessity for expanding mooring observations using underwater electronic holographic cameras such as those described by Sun et al. (2007).

67.12 DVM seasonal cycle, sea-ice cover, and suspended particles

It appears that DVM is triggered once the estimated near-surface illuminance falls below the 0.1-lux threshold (Figures 7 and 8). This suggests that the diurnal movement of zooplankton toward the surface at dusk starts once the near-

surface illuminance decreased to ~0.1 lux, and descends back the next morning before dawn as soon as the near-surface illuminance exceeds 0.1 lux. DVM follows changes in seasonal day length, and it stops at the sub-surface layer as soon as near-surface illuminance retains above ~0.1 lux for 24 h a day (Figures 7~~6~~b-7~~6~~g). At the CA13 latitude (71°21.356'N), the estimated value of near-surface or under-ice illuminance exceeds the 0.1 lux threshold for about 55~~12~~ and 50~~7~~ days before the midnight sun in 2004 and 2005, respectively (Figure ~~6~~7b). During fall 2004, the sub-surface DVM returned about 27~~0~~ days after the polar day season, once the midnight near-surface illuminance dropped below ~0.1 lux threshold around 2~~2~~8 August (Figures 6b-6g). Our results on the light threshold are consistent with the preferendum (isolume) hypothesis (e.g., Cohen and Forward, 2009). A variant of the preferendum hypothesis, the absolute intensity threshold hypothesis, suggests that an ascent at sunset is initiated once the light intensity decreases below a particular threshold level and a descent at sunrise occurs when the light intensity increases above the threshold intensity (e.g., Cohen and Forward, 2019). This is in line with our findings on an absolute 0.1-lux threshold of light, which corresponds to the moonlight illuminance at the gibbous moon during clear sky (Gaston et al., 2014).

The inter-annual variability in estimated under-ice illuminance is entirely attributed to the sea-ice thickness. During the ice season, the mean cloud cover (~40%) showed insignificant interannual variability (Figure ~~6~~7a); thus, the cloud cover was not taken into account. Our results reveal that sea-ice cover modifies the DVM seasonal cycle by attenuating under-ice illuminance. During winter-spring ~~Before the beginning of the polar day~~ 2004, CA13 was primarily covered with the first-year pack ice of about 1.6 m thick (Figures 3~~4~~b, 4 top, 5a, and 5b). In contrast, during the same time in 2005, ~~and likely during the entire winter 2004-2005,~~ the eastern Beaufort Sea continental slope was occupied by the multi-year pack ice of about 2.6 m thick (Figures ~~4~~3b~~c~~, 4 bottom~~d~~, 5c, and 5d). We suggest that this increased sea-ice thickness extended the DVM seasonal cycle toward the polar day of 2005. In May~~spring~~ 2005, the 0.1-lux threshold estimated for ~2.5~~6~~ m thick ice lags that for 2004 by about 5 days~~one week~~ (Figure 7~~6~~b). Following ice-diminished illuminance in April-May 2005, DVM at 28 m depth was ~~clearly~~ recorded until the beginning of~~7~~ May 2005. Moreover, DVM maintained integrity at 68-108 m depth until the open-water season started in mid-May 2005 (Figures 7~~6~~c and ~~6~~7e-~~6~~7g, respectively). In contrast, during spring 2004, DVM vanished about 1~~2~~0 and 28~~30~~ days ahead of the polar day and open-water season, respectively (Figures 7~~6~~). We suggest that this inter-annual DVM variability is consistent with under-ice illuminance. Its estimated value for mid-May 2004 (≥10 lux~~), Figure 6b)~~ exceeds that for May 2005 by a factor of 10 (Figure 7b~~not shown~~).

The MVBS actograms show asymmetry of the DVM seasonal cycle to the summer solstice (Figures 7~~6~~b-7~~6~~g). In summer 2004, the DVM seasonal cycle terminated about 54 days before the summer solstice but resumed, lagging summer solstice by 6~~1~~7 days. This asymmetry, being consistent with the estimated 0.1-lux threshold, is likely attributed to the seasonal sea-ice cover. During spring, the polar day begins when the eastern Beaufort Sea continental slope is still ice-covered (Figures 6a and 6b), which governs attenuation of light below the ice. In contrast, after the polar day is ended, the eastern Beaufort Sea continental slope remains ice-free or partly ice-covered until the end of October allowing sunlight to illuminate the near-surface water layer.

In the subsequent winters, the DVM backscatter intensity shows significant interannual variability. The dark-time MVBS during winter 2003-2004 exceeds that for winter 2004-2005 by ~ 3-5 dB (Figures ~~6~~7c-~~7~~6g). We attribute this inter-annual variability to attenuation of light by a thicker ice cover in winter 2004-2005, as follows from our preceding discussion. Satellite data and model simulations show ~~An assumption~~ that the eastern Beaufort Sea continental slope was occupied by Greenland pack ice during ~~the entire~~ winter-spring ~~2004~~ 2005 (Figures 4-6) that results in ~~leads to~~ the reduced estimate of under-ice illuminance by a factor of 10 (Figure 7b~~not shown~~). For example, during full moon events #6 and 7 in February-March 2005, the night-time moonlight illuminance felt down to the background night-time illuminance <0.0001 lux (Figure 7b).

In general, our results on the sea-ice impact on DVM show that DVM is well synchronized with the light/dark cycle modified by the sea-ice cover shading. It appears that thicker ice observed during winter 2004-2005 reduced the backscatter values (Figures ~~6~~7c-~~7~~6g), which likely demonstrates a light-mediated response of the zooplankton involved in DVM. This is in line with Berge et al. (2009) reporting a stronger polar night DVM in the ice-free Svalbard fjord compared to the ice-covered fjord. Vestheim et al. (2014) reported on shallowing DVM in Oslofjord in response to the freeze-up and subsequent snowfalls. They attributed this shallowing to a relative reduction of light intensities, which is similar to that observed over the eastern Beaufort Sea continental slope during winter-spring 2005. La et al. (2015) suggested that sea-ice diminishes DVM signals by blocking the detectable light intensity for DVM with depth during the Antarctic winter. At the same time, our results contrast with the observations of Wallace et al. (2010). They found no difference in time of the DVM onset and cessation between the seasonally ice-covered and ice-free Svalbard fjords, insisting on the role of the relative change in irradiance for triggering DVM. This discrepancy highlights an important difference between sea-ice in the Svalbard fjords and the eastern Beaufort Sea continental slope. Rijpfjorden in Svalbard is seasonally ice-covered with land-fast ice of ~0.8 m thick (Wallace et al., 2010). In contrast, in spring 2015 the eastern Beaufort Sea continental slope was occupied by 2.6 m thick multi-year Greenland pack ice (Figures 3b, and 4-6~~4d~~) favoring the synchronized DVM to extend toward the midnight sun.

Our data show that, during the midnight sun 2004, DVM ceased only at 28 m depth. In the underlying PW layer at 48-108 m depth, DVM continued until the beginning of July 2004 (Figures ~~7~~6c-~~7~~6e). However, DVM in the PW layer did not occur in phase with the 24-h light cycle. It seems that zooplankton was conducting regular synchronized DVM, but it was still avoiding relatively well-illuminated sub-surface water. This is in line with a predator-avoidance behavior during transitional seasons, but without seasonal modulation, because the sun is above the horizon 24 h a day. In fact, zooplankton limits DVM to the PSW water layer with relatively high chlorophyll fluorescence values during late summer (Figure 2). This can indicate high concentrations of phytoplankton (e.g., La et al., 2018), which zooplankton feeds on. The availability of phytoplankton can be an important factor triggering seasonal variability in DVM (e.g., La et al., 2015).

Usually, synchronized DVM stops during the midnight sun, consistent with a predator-avoidance behaviour of zooplankton conducting DVM (e.g., Blachowiak-Samolyk et al., 2006; Cottier et al., 2006; Wang et al., 2015; Darnis et al., 2017). However, Fortier et al. (2001) reported a clear midnight sun DVM in copepods under the spring ice of Barrow Strait at the centre of the Canadian Arctic Archipelago. They argued that absolute light intensity below sea ice decreases to the

thresholds at which the feeding activity of fish slows down. Moreover, DVM below 2-m thick ice in the Canada Basin during the midnight sun was recently reported by La et al. (2018). Following Fortier et al. (2001), we speculate that the absolute light intensity through the PW layer at CA13 was below the threshold of predators' perception allowing DVM during the midnight sun 2004. However, the midnight sun DVM was not obvious in 2005.

We suggest that the midnight sun DVM in 2005 was likely impacted~~masked~~ by the enhanced concentration of suspended particles through the PSW layer. Suspended particles return the ADCP acoustic signal, producing enhanced MVBS 24 h a day. For example, Petrusevich et al. (2020) reported on enhanced MVBS in Hudson Bay recorded by 300 kHz RDI Workhorse ADCP. They attributed this signal to the suspended particles released to the water column during ice melt. In contrast to the vertically synchronized DVM, suspended particles generated noise that can mask~~ed~~ DVM during the midnight sun 2005 as evident from Figures 7~~6~~d-7~~6~~f. On the CTD profile taken in September 2005, high particulate beam attenuation layers around 25 and 50 m depth match temperature maxima up to 1.3°C (Figure 2c). Moored CTD at 49 m depth shows several maxima up to 0.5°C following summer solstice 2005 (Figure 9~~8~~e). Two temperature maxima in the beginning and mid-June 2005 (Figure 9~~8~~e) match MVBS maxima at 68-88 m depth (Figure 7~~6~~f and 7~~6~~g). This suggests that MVBS maxima in actograms are generated by lateral advection of warm and turbid water layers. The formation of this water is likely attributed to wind-forced vertical mixing over the Beaufort Sea shelf involving surface riverine water heated by solar radiation and enriched with suspended particles. Alternatively, suspended particles can be attributed to resuspension of bottom sediments over the Beaufort Sea shelf. In any case, regardless of the source of suspended particles, their enhanced concentration in the water column during summer 2005 resulted in increased light attenuation (e.g., Hanelt et al., 2001), which potentially modified ~~disrupted~~ DVM during the midnight sun 2005.

6~~7~~.3~~2~~ DVM modifications by moonlight

In general, interpretation of the DVM modifications due to the moonlight is not straightforward. The dark-time MVBS in Figure 7c shows cumulative effect of sea-ice, cloud cover, water dynamics and moonlight. Individual events are often overlaid, and uncertainty in cloud cover also introduces an additional complication. Furthermore, during February-March, the moonlight below sea-ice is strongly attenuated (2004) or completely absorbed by sea-ice (2005) - Figure 3e. Moreover, under-ice vertical velocity data does not show DVM disruptions during full moon phases (Figure 8). However, ~~Our~~ MVBS actograms in Figures 7~~6~~c-7~~6~~g indicate modifications of DVM during a few days near the time of the full moon. These modifications are consistent with a lack of the upward moving zooplankton during the dark-time. They were observed from October to March including the civil twilight (Figures 7~~6~~b-7~~6~~g). The most pronounced moonlight modifications were observed during low cloud cover periods ~~attenuating the moonlight~~ (Figure 7~~6~~).

While our ~~The~~ results on the moon's modifications of DVM are not entirely conclusive, they are consistent with those previously reported for the Arctic and sub-Arctic regions. Moonlight plays a central role in structuring predator-prey interactions in the Arctic during the polar night below the ice (Last et al., 2016). It has been shown that during the polar night the moon's influence on DVM in the Arctic results in the zooplankton downward migration to deeper water for a few days

near the time of the full moon (Webster et al., 2015; Last et al., 2016). This is consistent with a concept that the moon phase cycle in the zooplankton migration is a global phenomenon in the ocean as suggested by Gliwicz (1986). As to DVM, the reason for the moon's modification was hypothesized to be a predator-avoidance behaviour against predators capable of utilizing the lunar illumination. Note, however, that during civil twilight 2005 below ~1~~2~~.8~~6~~ m thick pack ice, zooplankton responded to the estimated lunar illumination of 0.001 lux (Figures 7b and 7c~~not shown~~), which is far below the threshold of human and predators' perception. The moon's modification of DVM during the 2005 civil twilight suggests that zooplankton shows extraordinary sensitivity to illuminance (Båtnes et al., 2013; Cohen et al., 2015; Last et al., 2016; Petrusevich et al., 2016).

~~7~~6.43 DVM disruptions related to water dynamics

Our results revealed that water dynamics temporally impact DVM by disrupting the diurnal rhythm. Upwelling affects DVM the same way as moonlight forcing zooplankton to avoid the sub-surface water layer during the dark time of the day. In contrast, downwelling seems to force zooplankton to stay in the upper intermediate water layer (consisted of PSW) for 24 h a day. During downwelling, zooplankton likely avoids the lower intermediate layer comprised by PWW. The eddy disrupts DVM in the water layer below the eddy core inverting the MVBS diurnal signal. It seems that zooplankton prevents crossing the water layer occupied by the eddy core. The general impression is that zooplankton likely avoids enhanced water dynamics.

The characteristic feature of high-energetic events recorded at CA13 is the depth-dependent behavior of the horizontal flow. For upwelling and downwelling over the eastern Beaufort Sea continental slope, this feature is generated by the superposition of the background and wind-forced flow (Dmitrenko et al., 2018). The wind-driven barotropic flow generated by upwelling and downwelling wind forcing is superimposed on the background bottom-intensified shelfbreak current depicted by a dashed line in Figure 1~~0~~1c (Dmitrenko et al., 2018). For the downwelling storms, this effect amplifies the depth-intensified background circulation with enhanced PWW transport towards the Canadian Arctic Archipelago (Figure 11b and 11c, right). For the upwelling storms, the shelfbreak current is reversed, which results in surface-intensified flow moving in the opposite direction (Dmitrenko et al., 2018 and Figures 11a and 11c, left). The baroclinic eddies over the Beaufort Sea continental slope are likely explained by the shelfbreak current baroclinic instability (Spall et al., 2008).

It appears that upwelling, downwelling, and eddies disrupt DVM by generating a water layer with an enhanced gradient of horizontal velocity. We suggest that zooplankton avoids crossing this interface during diurnal migration, disrupting DVM. For crossing the high-gradient velocity layers, zooplankton has to spend additional energy. However, zooplankton is known for demonstrating a strategy of minimizing energy use while crossing water layers with enhanced water dynamics (Eiane et al., 1998; Basedow et al., 2004; Marcus and Scheef, 2009; Petrusevich et al., 2016, 2020; Cohen and Forward, 2019). For example, Petrusevich et al. (2016) reported on the DVM deviation in an ice-covered Northeast Greenland fjord in response to the estuarine-like circulation generated by a polynya opening over the fjord mouth (Dmitrenko et al., 2015). Overall, we suggest that in addition to the predator and starvation avoidance, the zooplankton beware to cross the high-gradient velocity layers remaining behind or below them, hence disrupting DVM.

It is suggested that upwelling and downwelling disrupt DVM. Zooplankton is transported offshore during upwelling and shoreward during downwelling (for review see Queiroga et al., 2007). For upwelling, the wind-driven Ekman offshore transport leads to offshore dispersal and wastage from coastal habitats. This is consistent with MVBS reduction recorded in the sub-surface layer during upwelling events (Figure ~~6~~7c). In fact, zooplankton can adjust migration strategy to avoid off-shore transport, reversing DVM (Poulin et al., 2002a,b). Moreover, zooplankton can avoid sweeping off-shore by upwelling and onshore by downwelling, maintaining preferred depth in the face of converging and downwelling flow (Shanks and Brink, 2005). DVM can be also impacted by the property of upwelled water. Huiwu et al. (2015) reported that DVM deviation is caused by aggregation of zooplankton in the upper 10-m layer in response to upwelling over the Chukchi Sea shelf northwest of the Alaskan coast. They explained DVM deviation by the nutrient-rich upwelled water, which favors an enhanced light attenuation by heavy phytoplankton. This, in turn, allows zooplankton to spend most of its time at the near-surface water layer.

We speculate that DVM disruptions attributed to upwelling and downwelling are primarily dominated by along-slope transport rather than the cross-slope transport. In addition to enhancing the cross-slope transport, upwelling and downwelling over the Beaufort Sea continental slope strongly modify along-slope transport through generating depth-dependent currents over the continental slope (Figure 11; Dmitrenko et al., 2016, 2018). We suggest that zooplankton avoids crossing horizontal velocity interface, generated by the superposition of wind-driven circulation and along-slope jet. This strategy is evident from the DVM disruption caused by the baroclinic eddy in February-March 2004. Below the depth of the maximum tangential speed (~90 m), DVM was found to be reversed (Figures 6g and 9). This is consistent with reversing DVM to avoid the upwelling induced off-shore Ekman transport in the Peru-Chile upwelling system (Poulin et al. 2002a,b). The reversed DVM in response to eddy passing clearly shows that zooplankton is capable to adjust its strategy of diurnal migration to avoid enhanced water dynamics.

~~7~~8 Conclusions

Based on the 2-year long time series from the mooring deployed over the upper eastern Beaufort Sea continental slope from October 2003 to September 2005, we conclude that the acoustic backscatter is dominated by DVM. DVM is controlled by the following different external forcings that also interplay.

(i) *Illuminance*. It is, in turn, controlled by the solar and moonlight cycling and sea-ice cover. The solar cycle controls DVM and its seasonal variability. In addition, sea-ice modifies seasonal patterns of DVM through light attenuation. A thicker multi-year Greenland pack ice present in winter-spring ~~2004~~ 2005 reduced the number of acoustic backscatters in the water column compared to that of winter-spring ~~2003~~ 2004 when the first-year pack ice dominated. Meanwhile, during spring 2005, the multi-year Greenland pack ice favored DVM prolongation toward the midnight sun due to the sea-ice shading the under-ice water layer. During civil twilight, the moon cycle generally modifies DVM, but this modification also depends on the sea-ice thickness and cloud cover. The strongest deviation was observed during mid-fall to early winter when sea ice is absent or relatively thin, and the NCEP-derived cloud cover is <30%. These deviations are associated with significant night-time

reduction of acoustic backscatters in the sub-surface layer. It seems that ~~Overall,~~ the full moon stimulates zooplankton to avoid the sub-surface layer.

(ii) *Water dynamics*. Upwelling and downwelling disrupt DVM. We found that this disruption is dominated by the along-slope water dynamics rather than the cross-slope Ekman transport. The surface-intensified along-slope flow generated by upwelling drives zooplankton to the lower intermediate depths hosting PWW to avoid the sub-surface layer. Zooplankton similarly respond to upwelling as it does to the moonlight. Thus, DVM disruptions induced by upwelling often interferes with the one generated by moonlight. In contrast, the bottom-intensified along-slope flow generated by downwelling modifies DVM through accumulating zooplankton in the upper intermediate layer occupied by PSW. The baroclinic eddy reverses DVM below the eddy core. We suggest that the zooplankton's response to upwelling, downwelling, and eddy is consistent with adjusting DVM to avoid enhanced water dynamics.

In contrast to many previous studies of the high-Arctic regions, at ~71°N latitude we recorded DVM during the midnight sun. During the ice-free season of the midnight sun 2004, DVM was observed through the PW layer. This DVM is likely limited by the depth of chlorophyll maxima in PSW. In 2005 the midnight sun DVM seemed to be masked by a high acoustic scattering level attributed to warmer and turbid layers observed through PSW.

Our analysis was limited by deficient zooplankton observations. ~~conducted around the location of the mooring in 2016 (Figure 1a). Zooplankton observations show that the large copepods *Calanus glacialis* and *Metridia longa* were performing DVM in September. However,~~ Aa comprehensive analysis of the scattering species comprising DVM is logistically impossible for the long-term deployments in the seasonally ice-covered and remote areas in the high Arctic. This prohibits identification of specific species whose DVM was detected by the 300 kHz ADCP and altered by the different environmental factors including illuminance and water dynamics.

Acknowledgments

The data used for this research were collected under the ArcticNet framework, project Long-Term Oceanic Observatories in the Canadian Arctic. ~~Camille Lafront at Université Laval did the taxonomic analysis of zooplankton in the selection of plankton net samples made for this study.~~ We gratefully acknowledge the support by the Canada Excellence Research Chair (CERC) and the Canada Research Chairs (CRC) programs. This work is a contribution to the joint Canadian-Danish-Greenland Arctic Science Partnership, Québec-Ocean, and the Canada Research Chair on the response of Arctic marine ecosystems to climate warming. The research was also partly supported by the National Sciences and Engineering Research Council of Canada (IAD: grant RGPIN-2014-03606, JKE: grant RGPIN/435373-2013).

Data

The ADCP data are available through the Polar Data Catalogue at https://www.polardata.ca/pdcsearch/, CCIN Reference #11653 (Gratton et al., unpublished).

Authors' contributions

Contributed to conception and design: IAD, VP, GD, SR, DB

Contributed to acquisition of data: JKE, AK, GD, AF, LF

Contributed to analysis and interpretation of data: IAD, VP, AK, GD, SK

Drafted and/or revised the article: IAD, VP, AK, GD, SR

Approved the submitted version for publication: IAD

References

Barber, D.G, Hop, H., Mundy, C.J., Else, B., Dmitrenko, I.A., Tremblay, J.-E., Ehn, J.K., Assmy, P., Daase, M., Candlish, L.M., and Rysgaard, S.: Selected physical, biological and biogeochemical implications of a rapidly changing Arctic Marginal Ice Zone, Prog. Oceanogr., 139, 122–150, doi:10.1016/j.pocean.2015.09.003, 2015.

Basedow, S., Eiane, K., Tverberg, V. and Spindler, M.: Advection of the zooplankton in an Arctic fjord (Kongsfjorden, Svalbard), Estuarine Coastal Shelf Sci., 60(1), 113–124, doi:10.1016/j.ecss.2003.12.004, 2004.

Båtnes, A. S., Miljeteig, C., Berge, J., Greenacre, M., and Johnsen, G.: Quantifying the light sensitivity of Calanus spp. during the polar night: potential for orchestrated migrations conducted by ambient light from the sun, moon, or aurora borealis?, Polar Biol., 1, 15, doi: 10.1007/s00300-013-1415-4, 2013.

Berge, J., Renaud, P.E., Darnis, G., Cottier, F., Last, K., Gabrielsen, T.M., Johnsen, G., Seuthe, L., Weslawski, J.M., Leuc, E., Moline, M., Nahrgang, J., Søreide, J.E., Varpeb, Ø., Lønne, O.J., Daasea, M., and Falk-Petersen, S.: In the dark: A review of ecosystem processes during the Arctic polar night, Prog. Oceanogr., 139, 258–271, doi:10.1016/j.pocean.2015.08.005, 2015.

~~Berge., J, Cottier, F., Varpe, Ø., Renaud, P.E., Falk-Petersen, S., Kwasniewski, S., Griffiths, C., Søreide, J.E. et al., Arctic complexity: a case study on diel vertical migration of zooplankton, J. Plankton Res., 36, 1279-1297, doi: 10.1093/plankt/fbu059, 2014.~~

Berge J., Cottier, F., Last, K.S., Varpe, Ø., Leu, E., Søreide, J., Eiane, K., Falk-Petersen, S., Willis, K., Nygård, H., Vogedes, D., Griffiths, C., Johnsen, G., Lorentzen, D., and Brierley, A.S., Diel vertical migration of Arctic the zooplankton during the polar night, Biol. Lett., 5, 69–72, doi: 10.1098/rsbl.2008.0484, 2009.

Brierley, A.S., Brandon, M.A., and Watkins, J.L., An assessment of the utility of an acoustic Doppler current profiler for biomass estimation, Deep Sea Res. Part I, 45(9), 1555–1573, doi: 10.1016/S0967-0637(98)00012-0, 1998.

Brierley, A.S., Diel vertical migration, Curr. Biol., 24, R1074−R1076, doi: 10.1016/j.cub.2014.08.054, 2014.

Chassignet, E.P., Hurlburt, H.E., Smedstad, O.M., Halliwel, G.R., Hogan, P.J., Wallcraft, A.J., Baraille, R., and Bleck, R., The HYCOM (Hybrid Coordinate Ocean Model) data assimilative system, Journal of Marine Systems, 65, 60–83, doi: 10.1016/j.jmarsys.2005.09.016, 2007.

Cohen, J.H., Berge, J., Moline, M.A., Sørensen, A.J., Last, K., Falk-Petersen, S., Renaud, P.E., Leu, E.S., Grenvald, J., Cottier, F., Cronin, H., Menze, S., Norgren, P., Varpe, Ø., Daase, M., Darnis, G., and Johnsen, G., Is Ambient Light during the High

Arctic Polar Night Sufficient to Act as a Visual Cue for Zooplankton?, PLoS ONE, 10(6), e0126247, doi: 10.1371/journal.pone.0126247, 2015.

Cavalieri, D.J., Markus, T., and Comiso, J.C., AMSR-E/Aqua Daily L3 12.5 km Brightness Temperature, Sea Ice Concentration, & Snow Depth Polar Grids, Version 3. Boulder, Colorado USA. NASA National Snow and Ice Data Center Distributed Active Archive Center, doi: 10.5067/AMSR-E/AE_SI12.003, 2014.

Cohen, J.H., and Forward, R.B., Zooplankton Diel Vertical Migration - A Review Of Proximate Control, Oceanography and marine biology: An Annual Review, 47, 77-109, 2009.

Cohen, J.H., and Forward, R.B., Vertical Migration of Aquatic Animals, Encyclopedia of Animal Behavior (Second Edition), Elsevier, 546-552, doi: 10.1016/B978-0-12-809633-8.01257-7, 2019.

Cottier F.R., Tarling, G.A., Wold, A., and Falk-Petersen, S., Unsynchronised and synchronised vertical migration of the zooplankton in a high Arctic fjord, Limnol. Oceanogr., 51, 2586–2599, doi: 10.4319/lo.2006.51.6.2586, 2006.

~~Daase, M., Eiane, K., Aksnes, D.L., and Vogedes, D., Vertical distribution of *Calanus* spp. and *Metridia longa* at four Arctic locations, Mar. Biol. Res., 4, 193–207, doi: 10.1080/17451000801907948, 2008.~~

Darnis, G., Hobbs, L., Geoffroy, M., Grenvald, J.C., Renaud, P.E., Berge, J., Cottier, F., Kristiansen, S., Daase, M., Søreide, J.E., Wold, A., Morata, N., and Gabrielsen, T., From polar night to midnight sun: Diel vertical migration, metabolismand biogeochemical role of the zooplankton in a high Arctic fjord (Kongsfjorden, Svalbard), Limnol. Oceanogr., 62, 1586–1605, doi: 10.1002/lno.10519, 2017.

Deines, K.L., Backscatter estimation using Broadband acoustic Doppler current profilers, in Proceedings of the IEEE Sixth Working Conference on Current Measurement (Cat. No.99CH36331), pp. 249–253, IEEE, San Diego, Calif, 1999.

Dmitrenko, I.A., Kirillov, S.A., Myers, P.G., Forest, A., Tremblay, B., Lukovich, J.V., Gratton, Y., Rysgaard, S., and Barber, D.G., Wind-forced depth-dependent currents over the eastern Beaufort Sea continental slope: Implications for Pacific water transport, Elem. Sci. Anth., 6, 66, doi: 10.1525/elementa.321, 2018.

Dmitrenko, I.A., Kirillov, S.A., Forest, A., Gratton, Y., Volkov, D.L., Williams, W.J., Lukovich, J.V., Belanger, C., and Barber, D.G., Shelfbreak current over the Canadian Beaufort Sea continental slope: Wind-driven events in January 2005, J. Geophys. Res., 121(4), 2447-2468, doi: 10.1002/2015JC011514, 2016.

Dmitrenko, I.A., Kirillov, S.A., Rysgaard, S., Barber, D.G., Babb, D.G., Pedersen, L.T., Koldunov, N.V., Boone, W., Crabeck, O., and Mortensen, J., Polynya impacts on water properties in a Northeast Greenland Fiord, Estuarine Coastal Shelf Sci., 153, 10–17, doi:10.1016/j.ecss.2014.11.027, 2015,

Dmitrenko, I.A., Wegner, C., Kassens, H., Kirillov, S.A., Krumpen, T., Heinemann, G., Helbig, A., Schröder, D., Hölemann, J.A., Klagge, T., Tyshko, K.P., and Busche, T., Observations of supercooling and frazil ice formation in the Laptev Sea coastal polynya, J. Geophys. Res., 115, C05015, doi: 10.1029/2009JC005798, 2010.

Dmitrenko, I.A., Kirillov, S.A., Ivanov, V.V., and Woodgate, R.A., Mesoscale Atlantic water eddy off the Laptev Sea continental slope carries the signature of upstream interaction, J. Geophys. Res., 113, C07005, doi: 10.1029/2007JC004491, 2008.

Eiane, K., Aksnes, D., and Ohman, M., Advection and the zooplankton fitness, SARSIA, 83, 87–93, doi: 10.1080/00364827.1998.10413674, 1998.

Falk-Petersen, S., Leu, E., Berge, J., Kwasniewski, S., Nygårdb, H., Røstad, A., Keskinen, E., Thormar, J., Quillfeldt, C., Wold, A., and Gulliksen, B., Vertical migration in high Arctic waters during autumn 2004, Deep Sea Res., Part II, 55(20-21), 2275–2284, doi: 10.1016/j.dsr2.2008.05.010, 2008.

Fielding, S., Griffiths, G., and Roe, H.S.J., The biological validation of ADCP acoustic backscatter through direct comparison with net samples and model predictions based on acoustic-scattering models, ICES J. Mar. Sci. J. du Cons., 61(2), 184–200, doi: 10.1016/j.icesjms.2003.10.011, 2004.

Fortier, M, Fortier, L., Hattori, H., Saito, H., and Legendre, L., Visual predators and the diel vertical migration of copepods under Arctic sea ice during the midnight sun, J. Plankton Res., 23, 1263–1278, doi: 10.1093/plankt/23.11.1263, 2001.

Gaston, K.J., Duffy, J.P., Gaston, S., Bennie, J., and Davies, T.W., Human alteration of natural light cycles: causes and ecological consequences, Oecologia, 176, 917–931, doi: 10.1007/s00442-014-3088-2, 2014.

Gliwicz, Z.M., A Lunar Cycle in The Zooplankton, Ecology, 67(4), 883-897, doi: 10.2307/1939811, 1986.

Gratton, Y, Ingram, G., Carmack, E., Van Hardengerget, B., Forest, A., Fortier, L., Blondeau, S., Massot, P., and Michaud, L., Long-term oceanic observatories (moorings) in the Beaufort Sea during the Canadian Arctic Shelf Exchange Study, 2002–2004, doi: 10.5884/11653, unpublished.

Grenfell, C.G., and Maykut, G.A., The optical properties of ice and snow in the Arctic Basin, J. Glaciol., 18(80), 445–463, doi: 10.3189/S0022143000021122, 1977.

Grenvald, J.C., Callesen, T.A., Daase, M., Hobbs, L., Darnis, G., Renaud, P.E., Cottier, F., Nielsen, T.G., and Berge, J., Plankton community composition and vertical migration during polar night in Kongsfjorden, Polar Biology, 39, 1879–1895, doi: 10.1007/s00300-016-2015-x, 2016.

Hanelt, D., Tüg, H., Bischof, K., Groß, C., Lippert, H., Sawall, T., and Wiencke, C., Light regime in an Arctic fjord: a study related to stratospheric ozone depletion as a basis for determination of UV effects on algal growth, Marine Biology, 138(3), 649–658, doi: 10.1007/s002270000481, 2001.

Hays G.C., A review of the adaptive significance and ecosystem consequences of the zooplankton diel vertical migrations, Hydrobiologia, 503, 163–170, doi: 10.1023/B:HYDR.0000008476.23617.b0, 2003.

Hobbs, L., Cottier, F.R., Last, K.S., and Berge, J., Pan-Arctic diel vertical migration during the polar night, Mar. Ecol. Prog. Ser., 605, 61– 72, doi: 10.3354/meps12753, 2018.

Hunke, E.C., Viscous-plastic sea ice dynamics with the EVP model: linearization issues, Computational Physics, 170, 18–38, doi: 10.1006/jcph.2001.6710, 2001.

Kalnay, E., et al., The NCEP/NCAR 40-year reanalysis project, Bull. Am. Meteorol. Soc., 77, 437–471, doi: 10.1175/1520-0477(1996)077<0437:TNYRP>2.0.CO;2, 1996.

Kirillov, S, Dmitrenko, I., Tremblay, B., Gratton, Y., Barber, D., and Rysgaard, S., Upwelling of Atlantic Water along the Canadian Beaufort Sea continental slope: Favorable atmospheric conditions and seasonal and interannual variations, J. Climate, 29(12), 4509–4523, doi: 10.1175/JCLI-D-15-0804.1, 2016.

Kosobokova, K.N., Diurnal vertical distribution of Calanus Hyperboreus Kroyer and Calanus Glacialis Jaschnov in Central Polar Basin, Okeanologiya, 18(4), 722–728, 1978.

Krishfield, R.A., Proshutinsky, A., Tateyama, K., Williams, W.J., Carmack, E.C., McLaughlin, F.A., and Timmermans, M.-L., Deterioration of perennial sea ice in the Beaufort Gyre from 2003 to 2012 and its impact on the oceanic freshwater cycle, J. Geophys. Res. Oceans, 119, 1271–1305, doi: 10.1002/2013JC008999, 2014.

Kulikov, E.A., Carmack, E.C., and Macdonald, R.W., Flow variability at the continental shelf break of the Mackenzie Shelf in the Beaufort Sea, J. Geophys. Res., 103(C6), 12,725–12,741, doi: 10.1029/97JC03690, 1998.

Kwok, R., Cunningham, G.F., Zwally, H.J., and Yi, D., Ice, Cloud, and land Elevation Satellite (ICESat) over Arctic sea ice: Retrieval of freeboard, J. Geophys. Res., 112, C12013, doi: 10.1029/2006JC003978, 2007.

Kwok, R., Cunningham, G.F., Wensnahan, M., Rigor, I., Zwally, H.J., and Yi, D., Thinning and volume loss of the Arctic Ocean sea ice cover: 2003–2008, J. Geophys. Res., 114, C07005, doi: 10.1029/2009JC005312, 2009.

La, H.S., Shimada, K., Yang, E.J., Cho, K.-H., Ha, S.-Y., Jung, J., Min, J.-O., Kang, S.-H., and Ha, H.K., Further evidence of diel vertical migration of copepods under Arctic sea ice during summer, Mar. Ecol. Prog. Ser., 592, 283–289, doi: 10.3354/meps12484, 2018.

La, H.S., Ha, H.K., Kang, C.Y., Wåhlin, A.K., and Shin, H.C., Acoustic backscatter observations with implications for seasonal and vertical migrations of the zooplankton and nekton in the Amundsen shelf (Antarctica), Estuarine, Coastal and Shelf Sci., 152, 124-133, doi: 10.1016/j.ecss.2014.11.020, 2015.

Last, K.S., Hobbs, L., Berge, J., Brierley, A.S., and Cottier, F., Moonlight drives ocean-scale mass vertical migration of the zooplankton during the Arctic Winter, Curr. Biol., 26(2), 244–251, doi: 10.1016/j.cub.2015.11.038, 2016.

Leise, T.L., Indic, P., Paul, M.J., and Schwartz, W.J., Wavelet meets actogram, J. Biol. Rhythms, 28(1), 62–68, doi: 10.1177/0748730412468693, 2013.

Lemon, D.D., Gower, J.F.R., and Clarke, M.R., The acoustic water column profiler: a tool for long-term monitoring of zooplankton populations, In: MTS/IEEE Oceans 2001. An Ocean Odyssey, Conference Proceedings (IEEE Cat. No.01CH37295), Honolulu, HI, USA, pp. 1904-1909, vol.3, doi: 10.1109/OCEANS.2001.968137, 2001.

Lemon, D.D., Billenness, D., and Buermans, J., Comparison of acoustic measurements of zooplankton populations using an Acoustic Water Column Profiler and an ADCP, In: OCEANS 2008, Quebec City, QC, pp. 1-8, doi: 10.1109/OCEANS.2008.5152009, 2008.

Lemon, D., Johnston, P., Buermans, J., Loos, E., Borstad, G., and Brown, L., Multiple-frequency moored sonar for continuous observations of zooplankton and fish, In: 2012 Oceans, Hampton Roads, VA, pp. 1-6, doi: 10.1109/OCEANS.2012.6404918, 2012.

Liu, Y., and Key, J.R., Assessment of Arctic Cloud Cover Anomalies in Atmospheric Reanalysis Products Using Satellite Data, J. Climate, 29, 6065-6083, doi: 10.1175/JCLI-D-15-0861.1, 2016.

Lorke, A., Mcginnis, D.F., Spaak, P., and Wüest, A., Acoustic observations of zooplankton in lakes using a Doppler current profiler, Freshw. Biol., 49, 1280–1292, doi: 10.1111/j.1365-2427.2004.01267.x, 2004.

Marcus, N.H., and Scheef, L.P., Photoperiodism in Copepods, in Photoperiodism: The Biological Calendar, edited by Nelson, R.J., Denlinger, D.L., and Sommers, D.E., pp. 193–217, Oxford University Press, Oxford, U. K., 2009.

Madsen, K.S., Rasmussen, T.A.S., Ribergaard, M.H., and Ringgaard, I.M., High resolution sea ice modelling and validation of the Arctic with focus on south Greenland waters, 2004-2013, Polarforschung, 85(2), 101-105, doi: 10.2312/polfor.2016.006, 2015.

Markus, T. and Cavalieri, D., Snow Depth Distribution over Sea Ice in the Southern Ocean from Satellite Passive Microwave Data. In: Antarctic Sea Ice: Physical Processes, Interactions, and Variability, Antarctic Research Series, 74, 19-39. Washington, DC: American Geophysical Union, 1998.

Melling, H., Riedel, D.A., and Gedalof, Z., Trends in the draft and extent of seasonal pack ice, Canadian Beaufort Sea, Geophys. Res. Lett., 32, L24501, doi:10.1029/2005GL024483, 2005.

O'Brien, M.C., Melling, H., Pedersen, T.F., and Macdonald, R.W., The role of eddies and energetic ocean phenomena in the transport of sediment from shelf to basin in the Arctic, J. Geophys. Res., 116, C08001, doi: 10.1029/2010JC006890, 2011.

Ott, M.J., The accuracy of acoustic vertical velocity measurements: instrument biases and the effect of Zooplankton migration, Continental Shelf Research, 25, 243-257, doi: 10.1016/j.csr.2004.09.007, 2005.

Perovich, D.K., The optical properties of sea ice, CRREL Monogr., 96-1, 25, 1996.

Petrusevich, V.Y., Dmitrenko, I.A., Niemi, A., Kirillov, S.A., Kamula, C.M., Kuzyk, Z.Z.A., Barber, D.G., and Ehn, J.K., Impact of tidal dynamics on diel vertical migration of zooplankton in Hudson Bay, Ocean Science, 16, 337–353, doi: 10.5194/os-16-337-2020, 2020.

Petrusevich, V., Dmitrenko, I.A., Kirillov, S.A., Rysgaard, S., Falk-Petersen, S., Barber, D.G., Boone, W., and Ehn, J.K., Wintertime water dynamics and moonlight disruption of the acoustic backscatter diurnal signal in an ice-covered Northeast Greenland fjord, J. Geophys. Res. Oceans, 121, 4804–4818, doi: 10.1002/2016JC011703, 2016.

Pickart, R.S., Shelfbreak circulation in the Alaskan Beaufort Sea: Mean structure and variability, J. Geophys. Res., 109, C04024, doi: 10.1029/2003JC001912, 2004.

Pickart, R.S., Weingartner, T.J., Pratt, L.J., Zimmermann, S., and Torres, D.J., Flow of winter-transformed Pacific water into the western Arctic, Deep Sea Res., Part II, 52, 3175–3198, doi: 10.1016/j.dsr2.2005.10.009, 2005.

Pnyushkov, A., Polyakov, I.V., Padman, L., and Nguyen, A.T., Structure and dynamics of mesoscale eddies over the Laptev Sea continental slope in the Arctic Ocean, Ocean Sci., 14, 1329-1347, doi: 10.5194/os-14-1329-2018, 2018.

Poulin, E., Palma, A.T., Leiva, G., Narvaez, D., Pacheco, R., Navarrete, S.A., and Castilla, J.C., Avoiding offshore transport of competent larvae during upwelling events: The case of the gastropod Concholepas concholepas in Central Chile, Limnol. Oceanogr., 47(4), 1248–1255, doi: 10.4319/lo.2002.47.4.1248, 2002a.

Poulin, E., Palma, A.T., Leiva, G., Hernández, E., Martínez, P., Navarrete, S.A., and Castilla, J.C., Temporal and spatial variation in the distribution ofepineustonic competent larvae of *Concholepas concholepas* along the central coast of Chile, Mar. Ecol. Prog. Ser., 229, 95–104, doi: 0.3354/meps229095, 2002b.

Queiroga, H., Cruz, T., dos Santos, A., Dubert, J., Gonzalez-Gordillo, J.I., Paula, J., Peliz, A., and Santos, A.M.P., Oceanographic and behavioural processes affectinginvertebrate larval dispersal and supply in the westernIberia upwelling ecosystem, Progress in Oceanography, 74, 174–19, doi: 10.1016/j.pocean.2007.04.007, 2007.

Shanks, A.L., and Brink, L., Upwelling, downwelling, and cross-shelf transportof bivalve larvae: test of a hypothesis, Mar. Ecol. Prog. Ser., 302: 1–12, doi: 10.3354/meps302001, 2005.

Spreen, G., Kaleschke, L., and Heygster, G., Sea ice remote sensing using AMSR-E 89 GHz channels, J. Geophys. Res., 113, C02S03, doi: 10.1029/2005JC003384, 2008.

Schweiger, A., Lindsay, R., Zhang, J., Steele, M., Stern, H., Uncertainty in modeled arctic sea ice volume, J. Geophys. Res., doi: 10.1029/2011JC007084, 2011

Spall, M., Pickart, R., Fratantoni, P., and Plueddemann, A., Western Arctic shelfbreak eddies: Formation and transport, J. Phys. Oceanogr., 38, 1644–1668, doi: 10.1175/2007JPO3829.1, 2008.

Stanton, T.K., Wiebe, P.H., Chu, D., Benfield, M.C., Scanlon, L., Martin, L., and Eastwood, R.L., On acoustic estimates of zooplankton biomass, ICES J. Mar. Sci., 51(4), 505–512, doi: 10.1006/jmsc.1994.1051, 1994.

Sun H., Hendry, D.C., Player, M.A. and Watson, J., In Situ Underwater Electronic Holographic Camera for Studies of Plankton, IEEE Journal of Oceanic Engineering, 32(2), 373–382, doi: 10.1109/JOE.2007.891891, 2007.

Tran, D., Sow, M., Camus, L., Ciret, P., Berge, J., and Massabuau, J.-C., In the darkness of the polar night, scallops keep on a steady rhythm, Sci. Reports, 6, 32435, doi: 10.1038/srep32435, 2016.

van Haren, H., and Compton, T.J., Diel Vertical Migration in Deep Sea Plankton Is Finely Tuned to Latitudinal and Seasonal Day Length, PLoS One, 8(5), e64435, doi: 10.1371/journal.pone.0064435, 2013.

Vestheim, H., Røstad, A., Klevjer, T.A., Solberg, I., and Kaartvedt, S., Vertical distribution and diel vertical migration of krill beneath snow-covered ice and in ice-free waters, J. Plankton Res., 36(2), 503–512, doi: 10.1093/plankt/fbt112, 2014.

Wallace, M.I., Cottier, F.R., Berge, J., Tarling, G.A., Griffiths, C., and Brierley, A.S., Comparison of the zooplankton vertical migration in an ice-free and a seasonally ice-covered Arctic fjord: An insight into the influence of sea ice cover on the zooplankton behavior, Limnol. Oceanogr., 55(2), 831–845, doi: 10.4319/lo.2010.55.2.0831, 2010.

Wang, H., Chen, H., Xue, L., Liu, N., and Liu, Y., The zooplankton diel vertical migration and influence of upwelling on the biomass in the Chukchi Sea during summer, Acta Oceanologica Sinica, 34(5), 68–74, doi: 10.1007/s13131-015-0668-x, 2015.

Wang, X., Key, J., Kwok, R., and Zhang, J., Comparison of Arctic Sea Ice Thickness from Satellites, Aircraft, and PIOMAS Data, Remote Sens., 8, 713, doi: 10.3390/rs8090713, 2016.

Webster, C., Varpe, Ø., Falk-Petersen, S., Berge, J., Stübner, E., and Brierley, A., Moonlit swimming: Vertical distributions of macrothe zooplankton and nekton during the polar night, Polar Biol., 38(1), 75–85, doi: 10.1007/s00300-013-1422-5, 2015.

Weingartner, T., Cavalieri, D., Aagaard, K., and Sasaki, Y., Circulation, dense water formation, and outflow on the northeast Chukchi shelf, J. Geophys. Res., 103(C4), 7647–7661, doi: 10.1029/98JC00374, 1998.

Williams, W.J., Carmack, E.C., Shimada, K., Melling, H., Aagaard, K., Macdonald, R.W., and Ingram, R.G., Joint effects of wind and ice motion in forcing upwelling in Mackenzie Trough, Beaufort Sea, Cont. Shelf Res., 26, 2352–2366, doi: 10.1016/j.csr.2006.06.012, 2006.

Wood, T.M., and Gartner, J.W., Use of Acoustic Backscatter and Vertical Velocity to Estimate Concentration and Dynamics of Suspended Solids in Upper Klamath Lake, South-Central Oregon: Implications for Aphanizomenon flos-aquae, Scientific Investigations Report 2010–5203, U.S. Geological Survey, Reston, Virginia, 20 p., 2010.

Woodgate, R.A., Aagaard, K., and Weingartner, T.J., Monthly temperature, salinity, and transport variability of the Bering Strait through flow, Geophys. Res. Lett., 32, L04601, doi: 10.1029/2004GL021880, 2005.

Yi, D., and Zwally, H.J., Arctic Sea Ice Freeboard and Thickness, Version 1. Boulder, Colorado USA. NASA National Snow and Ice Data Center Distributed Active Archive Center, doi: 10.5067/SXJVJ3A2XIZT. 2009, updated 2014.

Zhang, J.L. and Rothrock, D.A., Modeling global sea ice with a thickness and enthalpy distribution model in generalized curvilinear coordinates“, Mon. Weather Rev., 131, 845-861, doi: 10.1175/1520-0493(2003)131<0845:MGSIWA>2.0.CO;2, 2003.

Figures

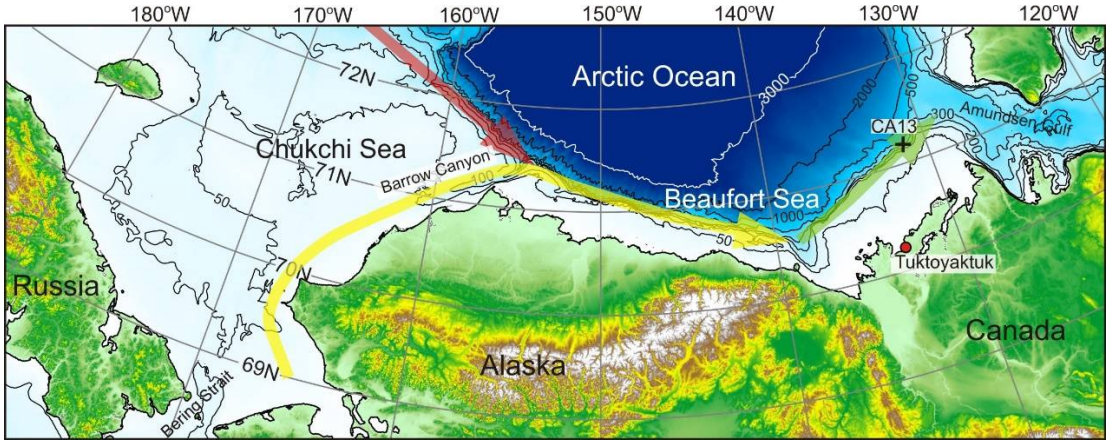

Figure 1: Map of the Beaufort Sea with the location of the ArcticNet mooring CA13 (black numbered cross). Thick red, yellow, and green arrows show circulation associated with the shelfbreak jet over the Chukchi Sea and western and eastern Beaufort Sea, respectively. ~~(**a**) Inset shows the position of stations with the zooplankton sampling identified by their station numbers and depicted by red crosses. Thin red arrows show directions to the zooplankton stations beyond the map limits.~~

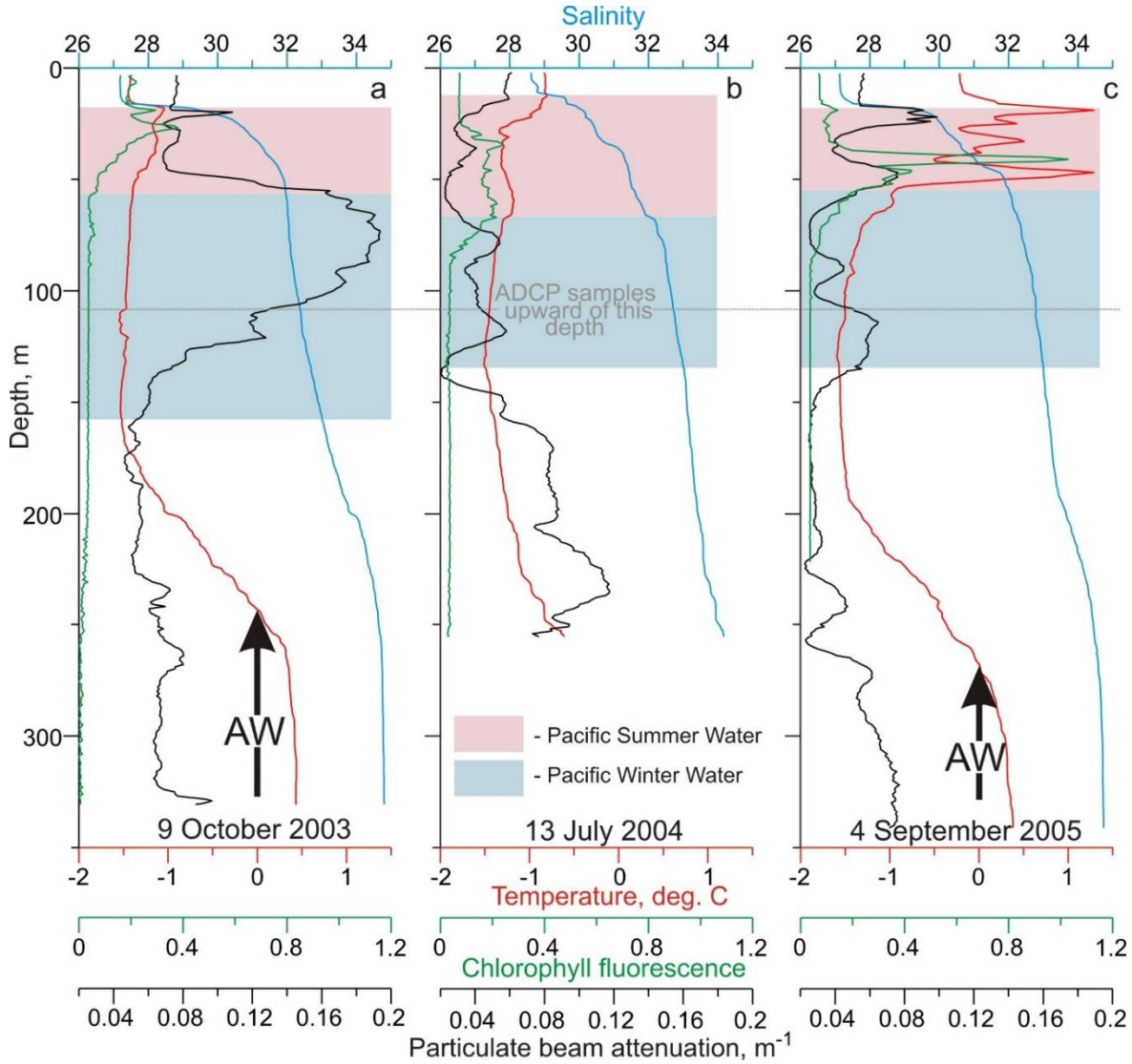

Figure 2: Vertical temperature (red), salinity (blue), chlorophyll fluorescence (green) and particulate beam attenuation (black) profiles taken at (**a**) mooring deployment on 9 October 2003, (**b**) on 13 July 2004 and (**c**) at mooring recovery on 4 September 2005. Pink and blue shading and black arrows highlight Pacific Summer Water (PSW), Pacific Winter Water (PWW), and Atlantic Water (AW), respectively, following Dmitrenko et al. (2016).

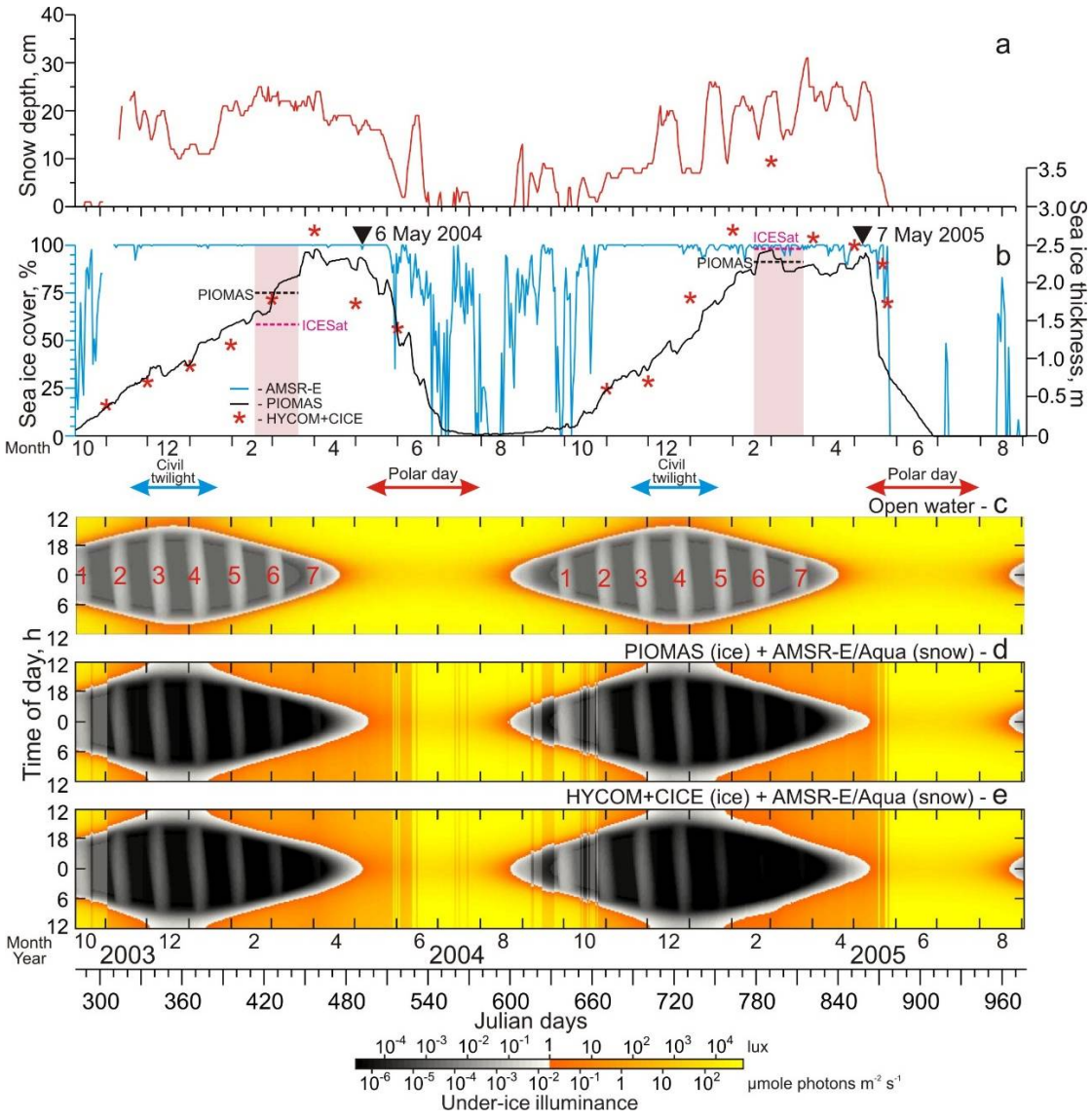

Figure 3: Time series of the (**a**) snow depth (cm, red), and (**b**) sea-ice concentrations (%, blue) and thickness ~~draft~~ (m~~, gray and black~~) from PIOMAS (black) and HYCOM+CICE (red stars). (**b**) Pink shedding highlights periods of two ICESat campaigns. Black and purple horizontal segments indicate the mean sea-ice thickness derived from PIOMAS and ICESat, respectively. ~~The sea-ice draft annual cycle shown for the first- and multi-year pack ice following Melling et al., 2005 (gray) and Krishfield et al., 2014 (black), respectively.~~ Black triangles at the top identify the time when the RADARSAT satellite images in Figure ~~5~~6 were acquired. (**c-e**) Actograms of under-ice illuminance modeled for (**c**) open water conditions, (**d,e**) snow from AMSR-E/Aqua, and sea-ice thickness from (**d**) PIOMAS and (**e**) HYCOM+CICE. Red and blue arrows at the top indicate the polar day and civil twilight, respectively. (**c**) Red numbers reference the full moon occurrences.

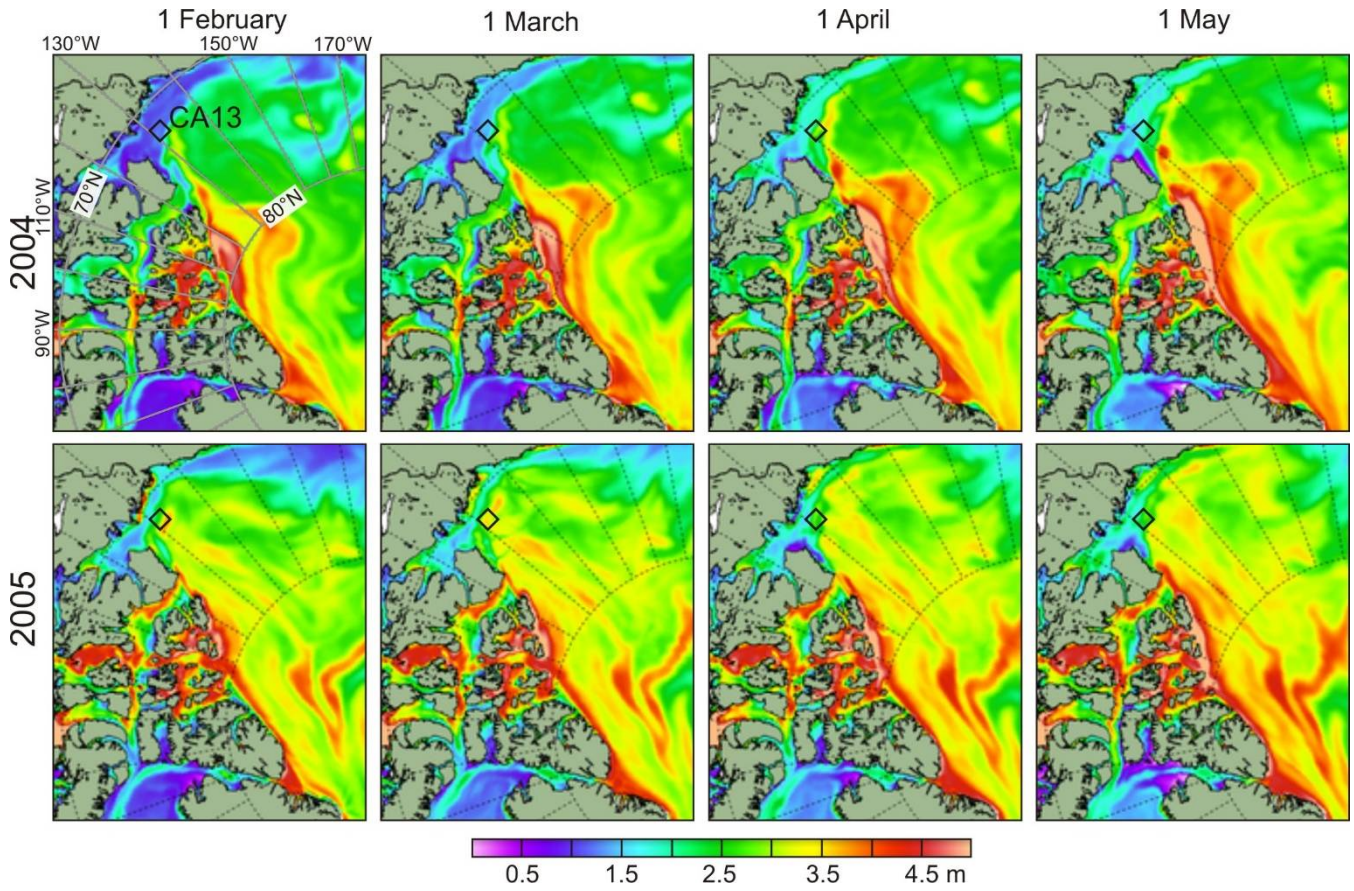

Figure 4: Spatial distribution of sea-ice thickness (m) based on model simulations using DMI's ocean and sea ice model HYCOM+CICE for February-May 2004 (top) and 2005 (bottom). The black diamonds depict mooring position.

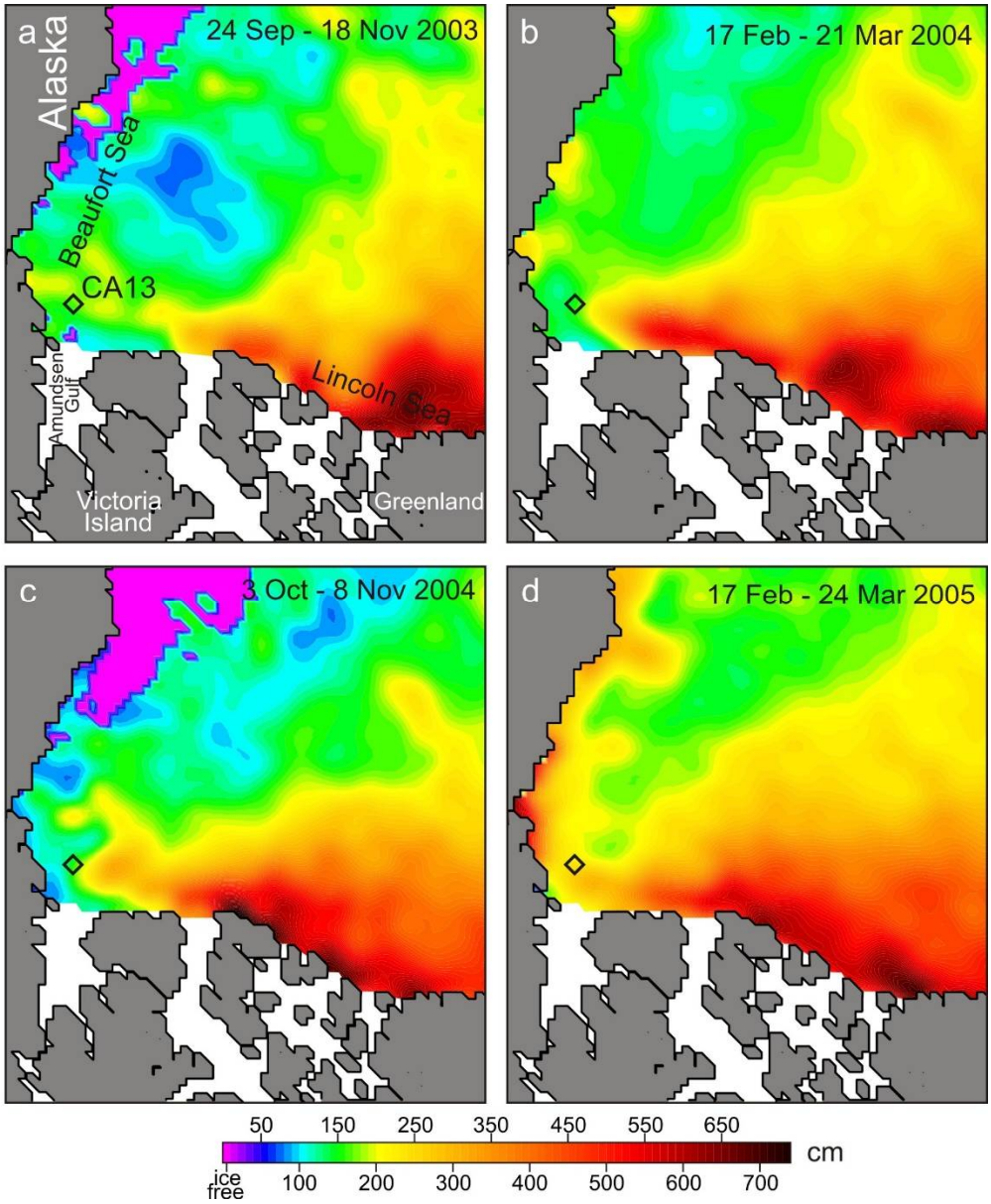

Figure 54: Spatial distribution of sea-ice thickness (cm) over the Canada Basin compiled using gridded sea ice thickness data from ICESat campaigns for (**a**) 24 September – 18 November 2003, (**b**) 17 February – 21 March 2004, (**c**) 3 October – 8 November 2004 and (**d**) 17 February – 24 March 2005 following Kwok et al. (2009). The black diamonds depict mooring position.

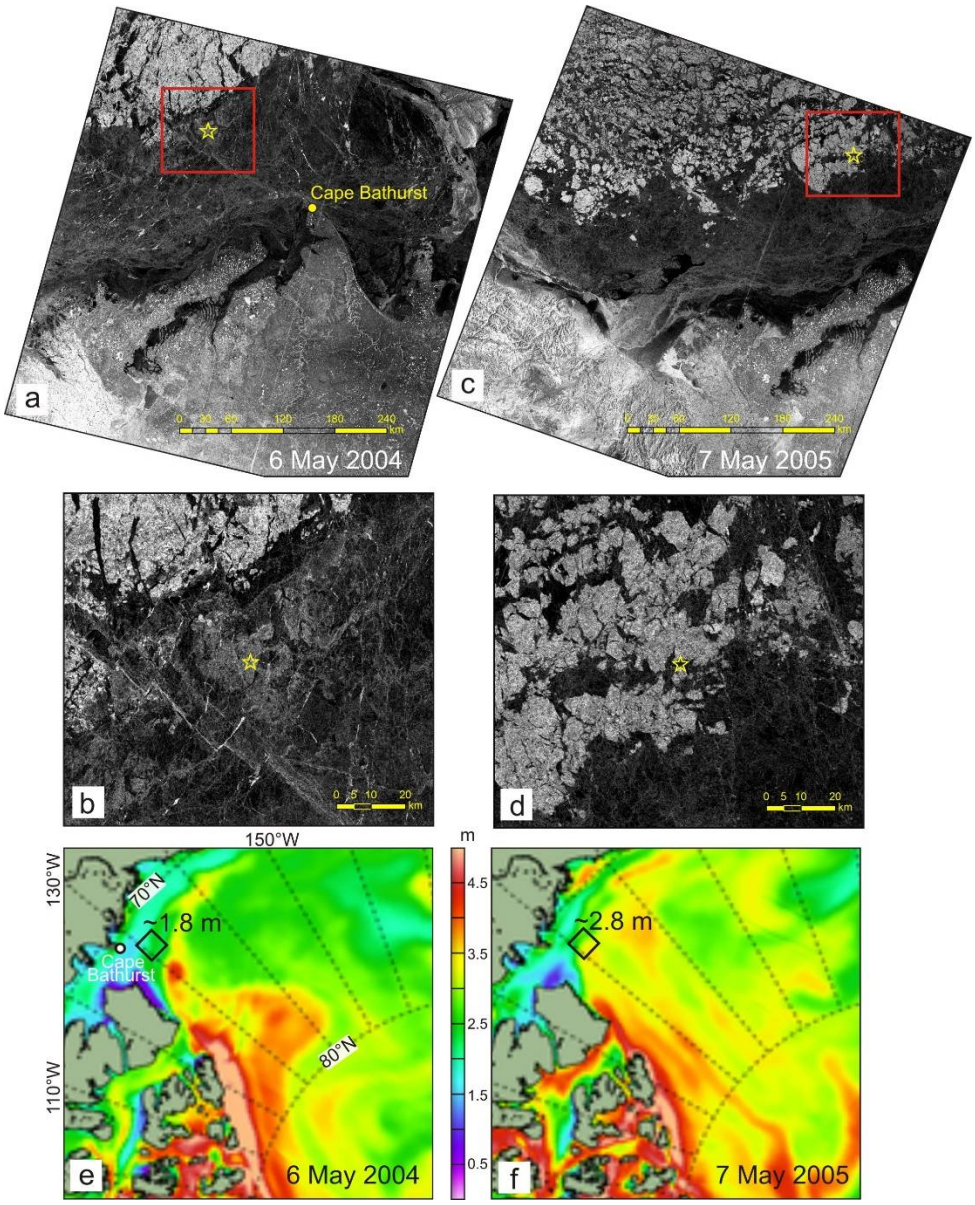

Figure 6~~5~~: (a-d) RADARSAT satellite images taken before sea-ice breakup over the CA13 location northeast of Cape Bathurst on (**a**) 6 May 2004 and (**c**) 7 May 2005. Red rectangles show mooring region enlarged in **b** and **d**. Yellow stars depict mooring position. The dark areas are associated with the first-year pack ice (< 2 m thick). The lighter areas indicate the multi-year pack ice (> 2 m thick). (**e-f**) Spatial distribution of sea-ice thickness (m) based on the HYCOM+CICE model simulations for (**e**) 6 May 2004 and (**f**) 7 May 2005. The black diamonds depict mooring position. Numbers show approximate sea-ice thickness.

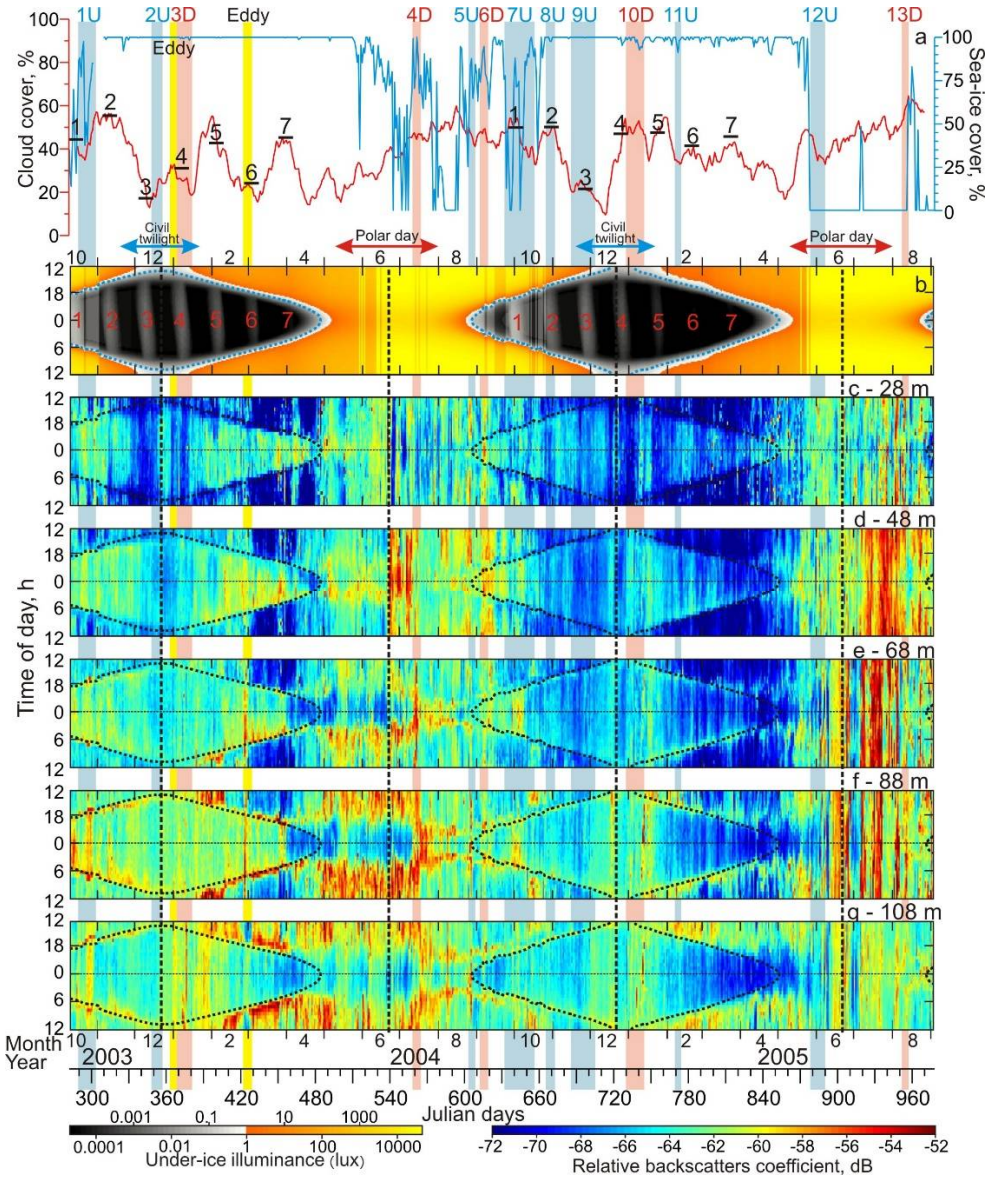

Figure 7~~6~~: (**a**) Time series of sea-ice concentrations (blue, %) and 15-day running mean of total cloud cover (red, %). Actograms of (**b**) modeled under-ice illuminance (lux) based on HYCOM+CICE sea-ice thickness, and (**c-g**) MVBS (dB) at five depth levels: (**c**) 28 m, (**d**) 48 m, (**e**) 68 m, (**f**) 88 m, and (**g**) 108 m. ~~(**b**) For January-April 2005, t~~The dotted blue (**b**) and black (**c-g**) lines depicts 0.1-lux threshold ~~estimated for 2.6 m thick ice~~. Red and blue arrows at the top indicate the polar day and civil twilight, respectively. Red numbers reference the full moon occurrences, and black horizontal segments in (**a**) indicate the mean cloud cover for these periods. Black dashed vertical lines depict solstices. Red and blue shading highlight the downwelling (D) and upwelling (U) events, respectively, with their reference numbers on the top. Yellow shading highlights eddies.

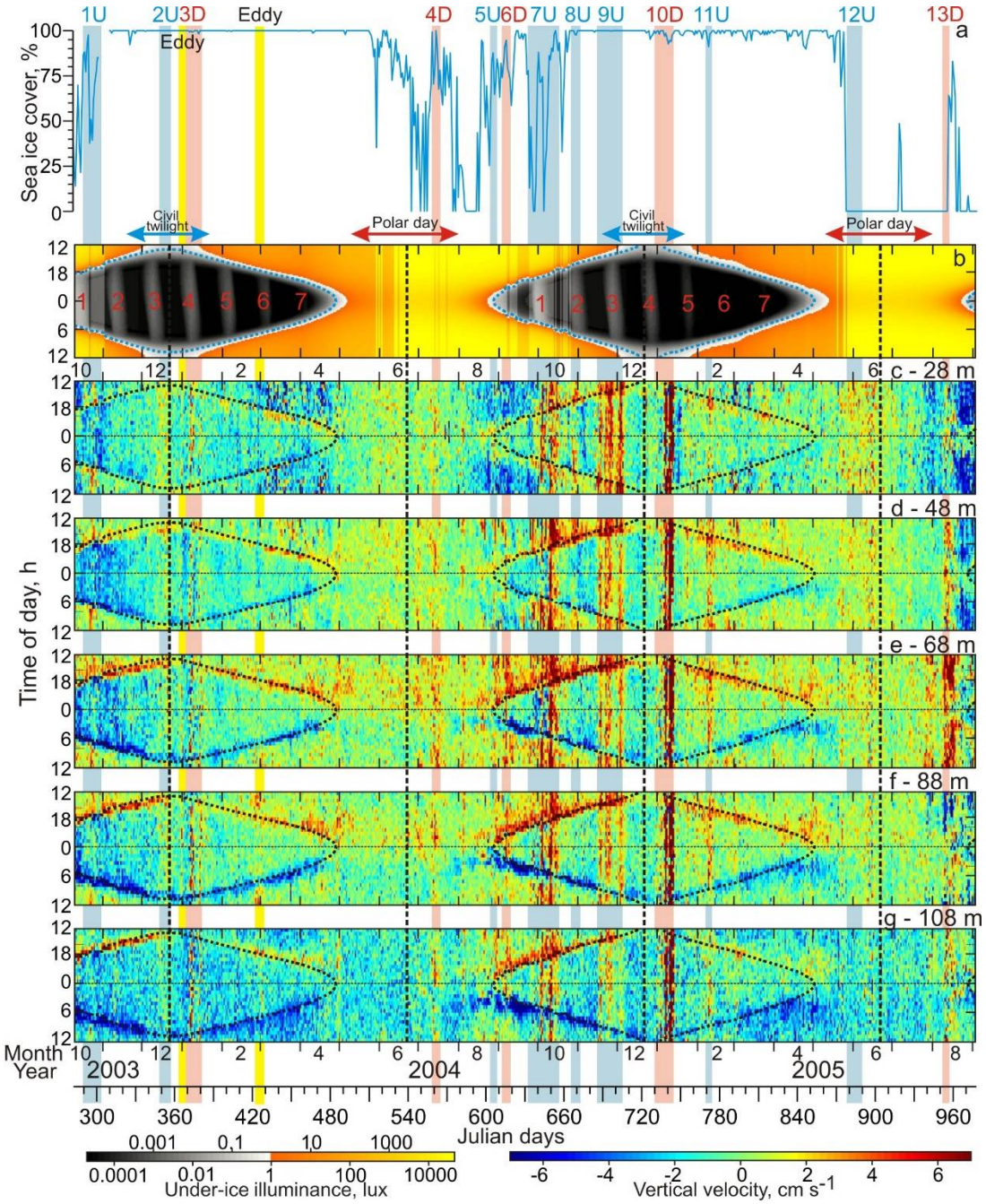

Figure 8~~7~~: (**a**) Time series of sea-ice concentrations (%). Actograms of (**b**) modeled under-ice illuminance (lux) based on HYCOM+CICE sea-ice thickness, and (**c-g**) ADCP-measured vertical velocity (cm s^{-1}) at five depth levels: (**c**) 28 m, (**d**) 48 m, (**e**) 68 m, (**f**) 88 m and (**g**) 108 m. Positive/negative values correspond to the upward/downward flow. All other designations are similar to those in Figure 7~~6~~.

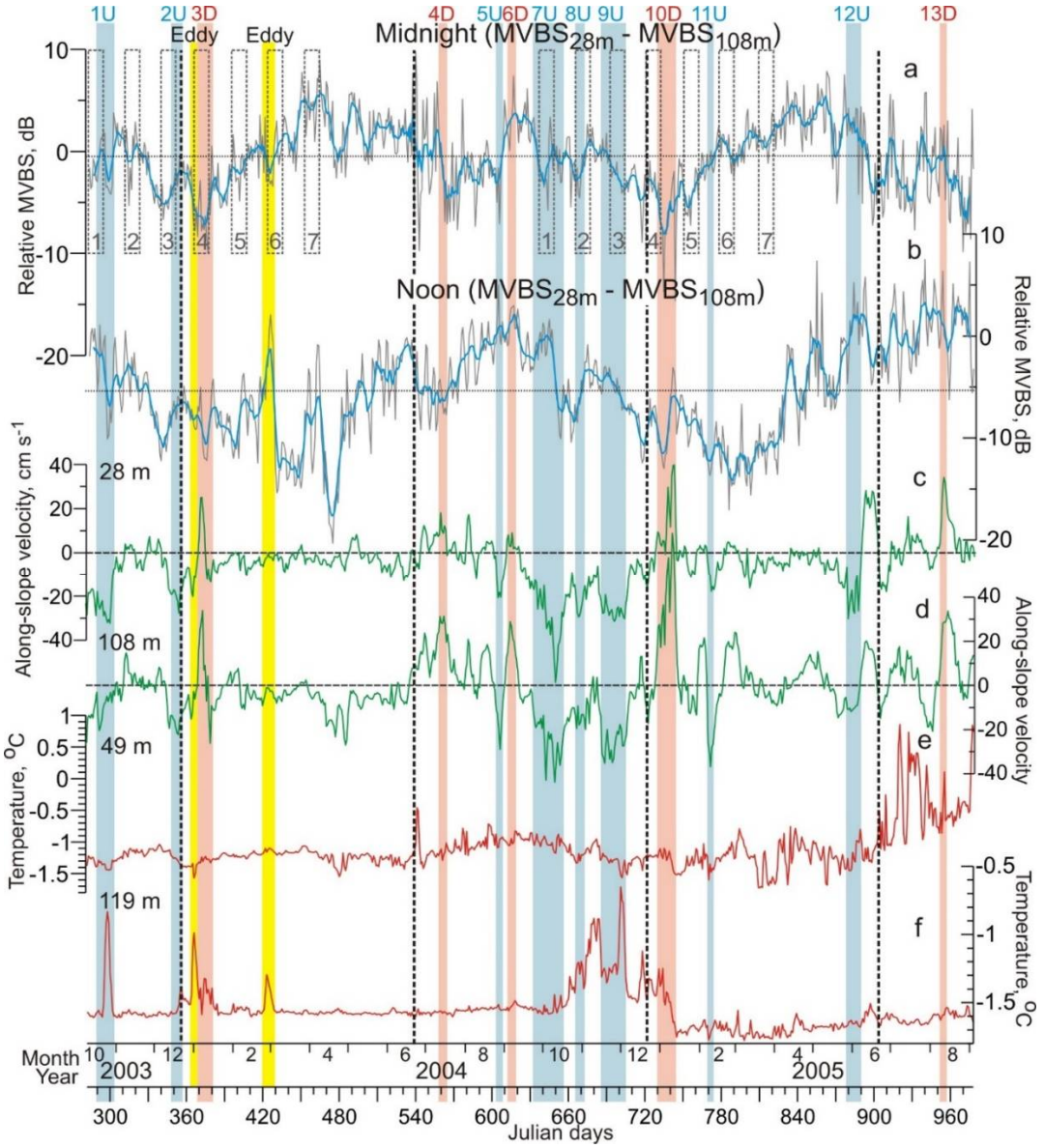

Figure 98: Time series of the daily mean relative MVBS (dB) from 28 m to 108 m depth for the astronomic (**a**) midnight and (**b**) noon ±1 h, along-slope (positive northeastward) velocity for depths of (**c**) 28 m and (**d**) 108 m (cm s^{-1}) and water temperatures (°C) for (**c**) 49 m and (**d**) 119 m depth. (**a-b**) Blue lines show the 7-day running mean. Horizontal dotted lines show the 2-year means. Positive/negative values correspond to MVBS gain/loss at 28/108 m depth. (**a**) Gray dashed rectangles depict the full moon occurrence ±6 days. All other designations are similar to those in Figure 76.

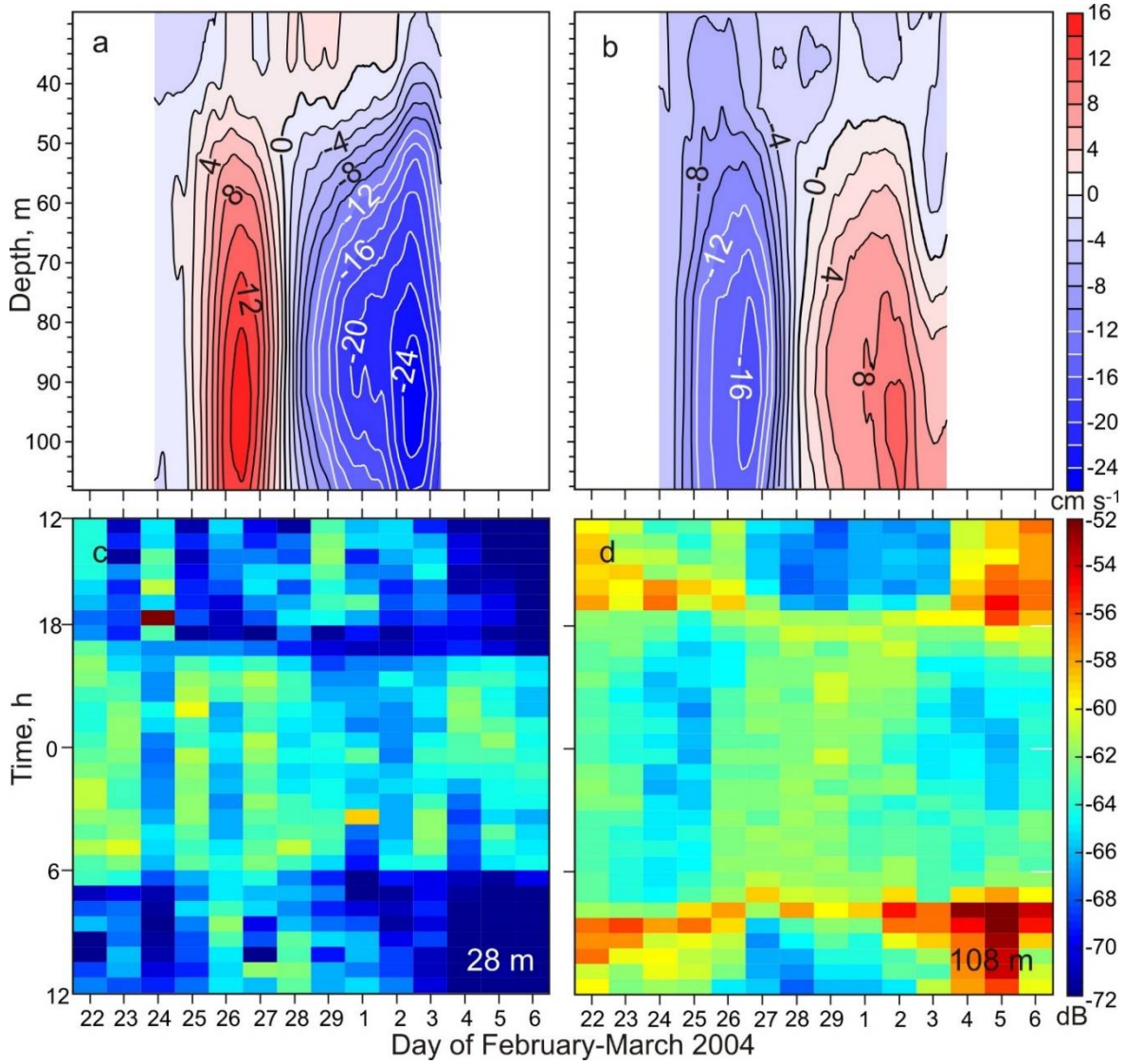

Figure 10: Enlarged view of the February-March 2004 eddy. (**a)** Zonal and (**b**) meridional current (cm s^{-1}) records as functions of depth adopted from Dmitrenko et al. (2018). (**c-d**) actograms of MVBS (dB) for (**c**) 28m and (**d**) 108 m depth.

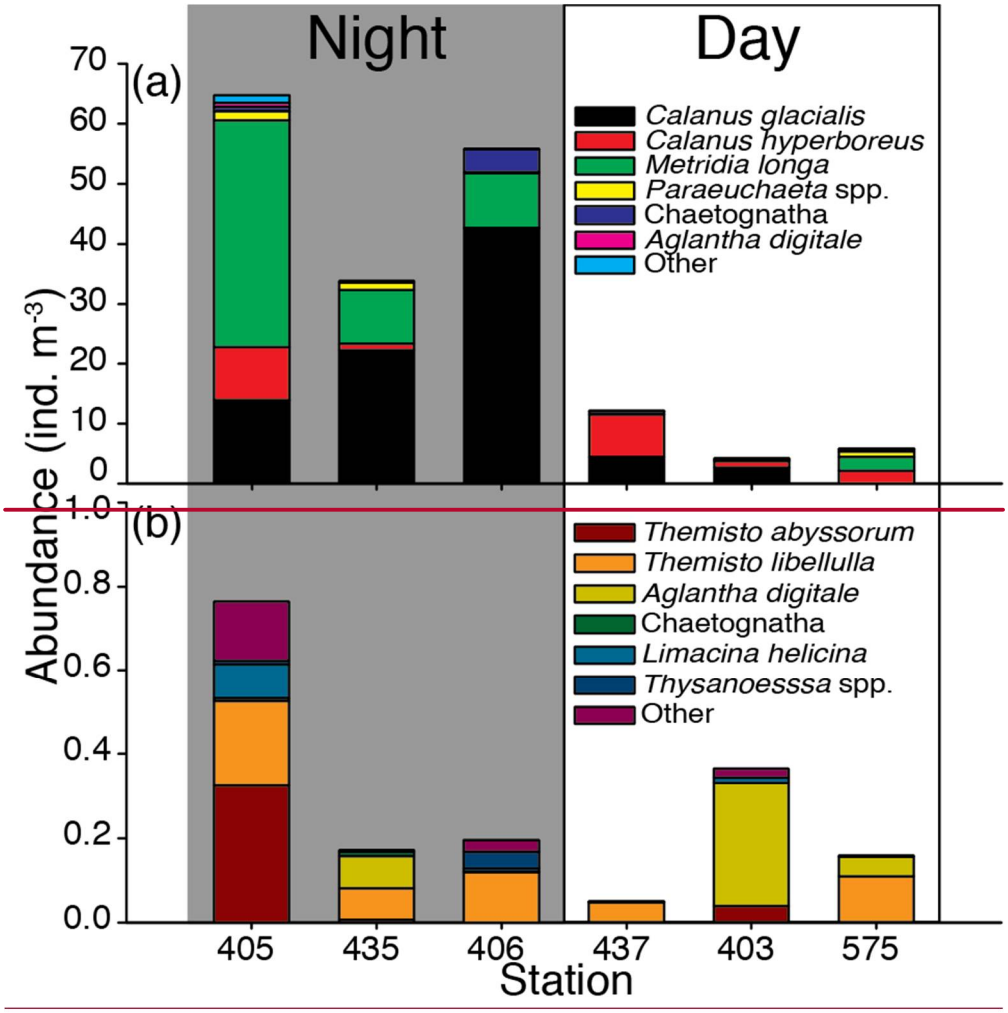

Figure 10: Large (**a**) mesozooplankton and (**b**) macrozooplankton numerical composition in the top 90-m layer of the water column during (left) night and (right) day time in the southeastern Beaufort Sea in the first half of September 2016. For station positions see Figure 1a.

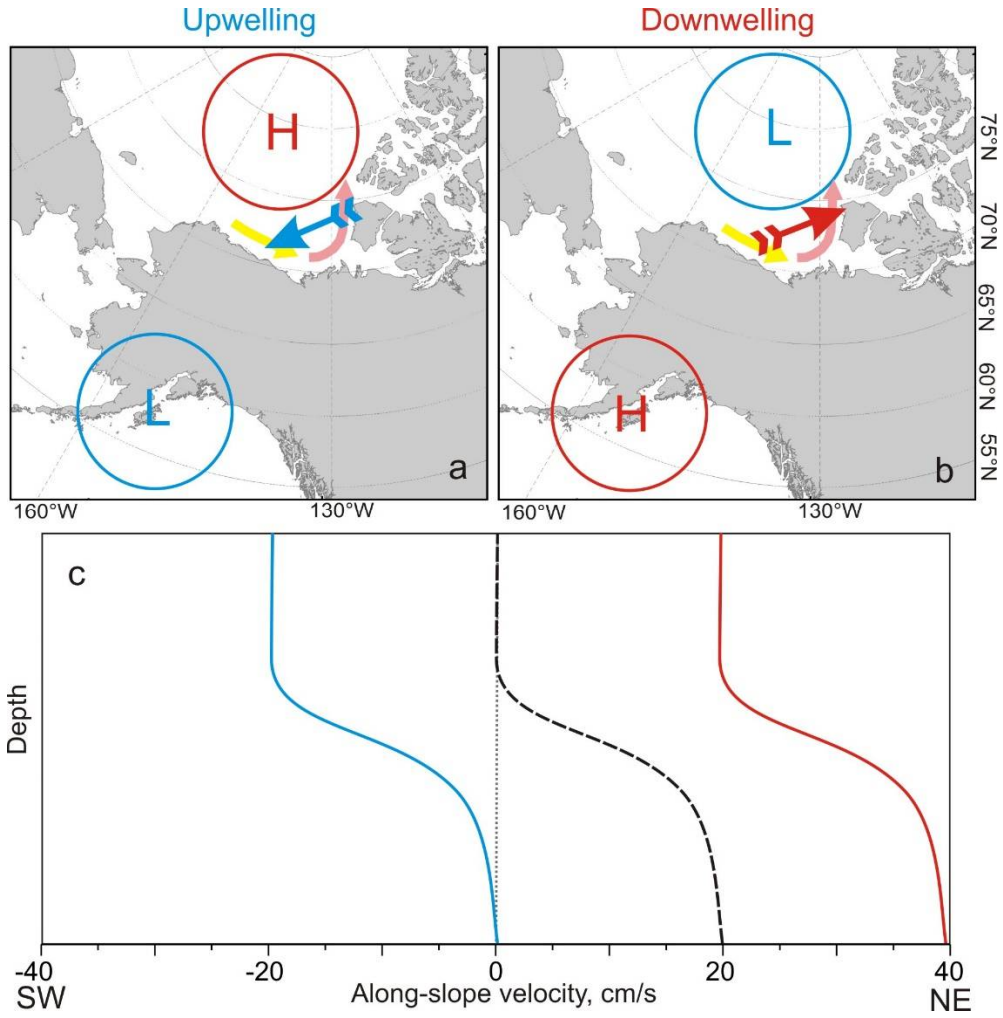

Figure 11: Schematic depiction showing atmospheric forcing for (**a**) upwelling and (**b**) downwelling along the eastern Beaufort Sea continental slope adopted from Kirillov et al. (2016). Blue and red arrows indicate geostrophic wind associated with concurrence between atmospheric low and high depicted by blue and red circles, respectively. Yellow and pink arrows show circulation with shelfbreak jet over the western and eastern Beaufort Sea, respectively, intensified by local downwelling. (**c**) Schematic depiction suggesting generation of the surface-intensified (blue curve) and depth-intensified (red curve) along-slope currents as a result of upwelling and downwelling, respectively, superimposed on the hypothetical bottom-intensified shelfbreak current (black dashed curve) following Dmitrenko et al. (2018).